

Multi-Network Constrained Operational Optimization in Community Integrated Energy Systems: A Safe Reinforcement Learning Approach¹

Ze Hu^a, Ka Wing Chan^{a,b*}, Ziqing Zhu^c, Xiang Wei^a, Siqi Bu^{a,b,d}

^a Department of Electrical and Electronic Engineering, The Hong Kong Polytechnic University, Hung Hom, Hong Kong SAR

^b Research Centre for Grid Modernisation, The Hong Kong Polytechnic University, Hung Hom, Hong Kong SAR

^c Department of Computer Science, The Hong Kong Baptist University, Kowloon Tung, Hong Kong SAR

^d International Centre of Urban Energy Nexus, The Hong Kong Polytechnic University, Hung Hom, Hong Kong SAR

Abstract:

The integrated community energy system (ICES) has emerged as a promising solution for enhancing the efficiency of the distribution system by effectively coordinating multiple energy sources. However, the operational optimization of ICES is hindered by the physical constraints of heterogeneous networks including electricity, natural gas, and heat. These challenges are difficult to address due to the non-linearity of network constraints and the high complexity of multi-network coordination. This paper, therefore, proposes a novel Safe Reinforcement Learning (SRL) algorithm to optimize the multi-network constrained operation problem of ICES. Firstly, a comprehensive ICES model is established considering integrated demand response (IDR), multiple energy devices, and network constraints. The multi-network operational optimization problem of ICES is then presented and reformulated as a constrained Markov Decision Process (C-MDP) accounting for violating physical network constraints. The proposed novel SRL algorithm, named Primal-Dual Twin Delayed Deep Deterministic Policy Gradient (PD-TD3), solves the C-MDP by employing a Lagrangian multiplier to penalize the multi-network constraint violation, ensuring that violations are within a tolerated range and avoid over-conservative strategy with a low reward at the same time. The proposed algorithm accurately estimates the cumulative reward and cost of the training process, thus achieving a fair balance between improving profits and reducing constraint violations in a privacy-protected environment with only partial information. A case study comparing the proposed algorithm with benchmark RL algorithms demonstrates the computational performance in increasing total profits and alleviating the network constraint violations.

Keywords: Integrated community energy system, optimal operation, integrated demand response, safe reinforcement learning

1. Introduction

1.1 Motivation

With global challenges posed by fossil energy depletion and climate change, the energy system is undergoing a profound transition worldwide [1]. This transition is accompanied by increased integration of diverse energy sources, leading to interconnected energy markets and growing complexities [2]. Notably, the demand side, primarily composed of community buildings, constitutes over 20% of energy consumption within the whole energy system [3]. In this context, integrated community energy system (ICES) emerges as a promising solution for efficient multi-energy coordination and utilization. It is particularly effective in dispatching demand flexibility to handle complex system operation and increasing renewable penetration [4]. Consequently, the operational optimization of ICES is crucial for integrating diverse energy transactions and enhancing overall energy efficiency [5].

1.2 Related work

Numerous studies have focused on ICES with multi-energy carrier coordination of power, gas, and heat. As one of the key topics in energy system operation, the demand response (DR), has been extended to integrated demand response (IDR) with the coordination of demand for multiple energy in ICES [6]. The application of IDR offers multiple advantages. By coordinating the demand for multiple energies, IDR can significantly increase energy utilization, thereby reducing the cost of multi-energy users (MEU) and improving the profits of the entire community [7]. IDR has also been employed in [8] to assist in peak shaving and valley filling in energy system operations. [9] and [10] have exploited the horizontal complementary substitution and vertical time shift strategy of IDR to realize robust operation. Furthermore, IDR accommodates renewable uncertainties from wind turbine (WT) and photovoltaic (PV), playing a crucial role in ICES operation [11]-[13]. While previous studies have explored IDR in multiple aspects, its functionality in ensuring safe operation accounting for multiple network constraints including electricity, natural gas, and heat, has not been thoroughly examined. In addition, IDR can provide cross-energy flexibility in multi-network operations, due to its strong spatiotemporal coupling characteristic in integrated energy systems. This endows IDR a significant potential in multi-network balancing of ICES for both economic profits and operational safety [14]. Therefore, this paper focuses on IDR in solving the multi-network constrained operational optimization problem in ICES.

Various works have been focused on solving the operational optimization of ICES, but existing literature considering the multi-network constraints is limited. The key challenge lies in handling the non-convex constraints of network and energy devices. A

¹The short version of the paper was presented at CUE2023. This paper is a substantial extension of the short version of the conference paper

common approach is mathematical programming. Reference [15] examines the interaction between an integrated system operator and its multiple integrated load aggregators. All network constraints are relaxed by second-order cone relaxation, and the non-convex features are improved by the McCormick method. The problem is then reformulated into mixed integer linear programming (MILP), which can be solved by commercial solvers. Reference [16] establishes a two-stage model that considers the detailed thermal inertia. The nonlinearity of the network constraints is tackled by the big-M method and piece-wise linearization, and the problem is reformulated to MILP based on Karush-Kuhn-Tucker (KKT) conditions and the strong duality theorem. However, these approaches are computationally expensive in linearization and convexification when dealing with non-linear or non-convex physical constraints of networks. The situation worsens when the non-convex operating characteristic of energy devices, such as combined heat and power (CHP), is considered [17]. Furthermore, protecting transaction privacy presents another significant challenge for mathematical programming approaches [18].

Reinforcement Learning (RL) algorithms have garnered significant research attention for addressing optimization problems in recent years. By interacting with the external environment, RL algorithms empower intelligent agents to iteratively learn their optimal strategies with only partial environmental information. Specifically, RL has the advantages of generalization, exploration, and delayed consequences, as it can be widely implemented in various environments with dedicated Markov decision processes (MDP), improving strategies through ‘trial and error’, and learning the optimal strategy in environments with delayed or sparse reward. Moreover, by leveraging Deep Neural Networks (DNN) to estimate the value function, RL algorithms can facilitate continuous action spaces, and handle the increasing scalability and complexity of the environment. These RL algorithms with DNN, known as deep reinforcement learning (DRL), have found successful applications across diverse domains, including strategic games like Go [19], and Atari games [20], as well as energy system optimizations [21],[22]. For instance, [21] uses a model-free DRL algorithm, deep deterministic policy gradient (DDPG) to optimize the energy management of a PV-integrated energy hub. Similarly, the utilization of Distributed Proximal Policy Optimization (DPPO) and Soft Actor-Critic (SAC) algorithms optimizes the scheduling of islanded energy systems, accounting for multi-uncertainties and hydrothermal simultaneous transmission [22]. However, the conventional RL algorithms are designed to tackle unconstrained optimization problems, and their efficacies diminish when applied to constrained optimization problems. The lack of awareness regarding the network constraint violation strongly restricts the application of DRL algorithms in industrial practice [23], as it can lead to economic loss and even system blackout.

To address this challenge, Safe Reinforcement Learning (SRL) algorithms have been developed to solve constrained optimization problems. SRL approaches can be classified into three categories: i) Penalizing constraint violations in the reward function by adding a penalty term [24]. However, this requires choosing a suitable penalty value, which is a difficult and sensitive task that depends on the reward scale, the number and scale of constraints, and the degree of safety [25]. ii) Projecting unsafe actions to safe ones by solving a projection problem, for example, approximated Lyapunov constraints [26]. This method relies on a projection model, which is based on predefined DNNs or matrices with potentially large approximation errors [27]. Therefore, the resulting actions could be overly conservative. iii) Penalizing the constraint violations in the action-value function dynamically by introducing the Lagrangian multiplier, instead of using a fixed penalty value in the reward [28],[29]. The multiplier is stochastically updated as a dual variable of the policy during the agent training based on the cost value function. However, the Lagrangian method-based SRL algorithm may not converge to the optimal solution because of the cost value function overestimation.

1.3 Summary of contributions

In summary, three significant research gaps in the relevant literature have been identified to be addressed. First, most research overlooks the multi-network constraints in ICES. Violation of these constraints can compromise the economic value of the entire community, as well as the security and stability of the network within ICES. Second, current methods cannot fully handle the non-linearity and non-convexity of energy devices and network constraints. Approaches like mathematical programming not only require significant work in convexification and linearization but also need complete information for an accurate solution, which breaches the privacy protection in ICES. The conventional RL algorithm, however, on the other hand, performs poorly in multi-network constrained optimization due to its unawareness of constraints in optimization logistics. Third, existing SRL algorithms have multiple drawbacks, including difficulty in determining penalties for the direct penalization method, over-conservative policies for the Lyapunov method, and Q-value overestimation for the Lagrangian method. These problems result in an unfair tradeoff between the reward and cost during the training process, leading to severe constraint violations or conservative policies.

This paper presents a comprehensive ICES model that considers non-convex characteristics of energy devices and IDR. The multi-network models of integrated energy including electricity, natural gas, and heat, are established to constrain the ICES operation. As a result, a network-constrained optimization problem in the ICES model is formulated and then transformed into a constrained Markov decision process (C-MDP). To solve the C-MDP, a novel SRL algorithm, namely primal-dual twin delayed deep deterministic policy gradient (PD-TD3), is then proposed. This algorithm uses a Lagrangian multiplier to dynamically penalize the constraint violation, overcoming the drawback of the typical RL method in solving constrained optimization problems. Specifically, it introduces additional double Q networks to estimate Q-values for reward and cost, which not only alleviates the Q-value overestimation problem of typical SRL algorithms but leads to a fair tradeoff between improving the profits and reducing the constraint violation. Furthermore, the algorithm updates the policy and its dual variable with delay, which stabilizes the training process and helps converge to the global optimal.

The contributions of this paper are as follows:

- 1) A comprehensive model of ICES that coordinates electricity, natural gas, and heat, is proposed. In this model, the ICES provides integrated energy to meet the demand of MEUs in the community by converting energy locally and procuring energy from the wholesale market. Thus, the ICES needs to price for multi-energy without violating the privacy of MEUs, while MEUs with integrated energy flexibilities can adjust their energy consumption according to the price changes. Additionally, the ICES model accounts for non-linear physical characteristics of energy devices, which leads to a more efficient operation.
- 2) The proposed model takes into account the physical constraints of integrated energy networks within the ICES. These networks are foundational components and are vital for the efficient transmission and distribution of energy resources. Specifically, this network model captures the physical characteristics of energy flow and imposes security operational constraints for the distribution level energy transmissions in ICES operation.
- 3) A C-MDP is formulated from the constrained operational optimization problem for the ICES with multi-energy integration. Also, the physical constraint violations of integrated energy networks are considered as the cost in the C-MDP.
- 4) A novel safe DRL algorithm, namely PD-TD3, is proposed to solve the C-MDP and the constrained operational optimization problem of ICES. This algorithm maximizes the operational profits and minimizes the physical constraint violation simultaneously by employing the Lagrangian multiplier to penalize the cost for violations. The PD-TD3 algorithm can address the high-dimensional non-convex decision-making problem by using DNN to estimate the policy and action-value function. Furthermore, the use of a double Q network reduces the over-estimation problem of the action value for both the reward and cost, and the delayed update stabilizes the training process of policy and its dual variable. The PD-TD3 can find the optimal solution that balances the maximal profits and the lowest constraint violation.

The remaining paper is organized as follows. The mathematical models of ICES, including devices and MEUs, are presented in Section 2. The integrated network models for electricity, natural gas, and heat are detailed in Section 3. The constrained operational optimization problem and the corresponding C-MDP are formulated in Section 4. The novel SRL algorithm is proposed in Section 5 to solve the C-MDP. Finally, several cases are conducted to verify the algorithm performance and analyze the simulation result in Section 6. The whole paper is concluded in Section 7.

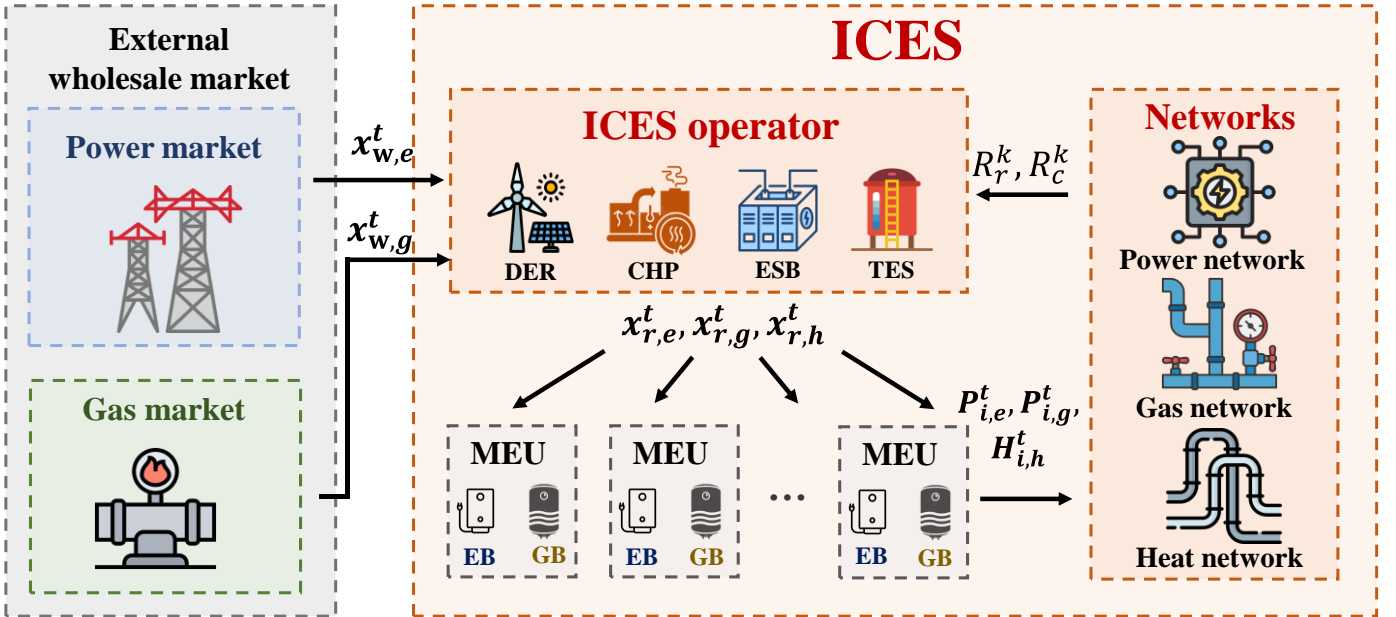


Fig.1. Illustration of the integrated community energy system

2. System modeling

This section focuses on a comprehensive ICES model, including various types of energy sectors and resources. Specifically, the ICES, as depicted in Fig.1, operates as a localized integrated energy system catering to MEUs on the demand side. The ICES consists of 1) two types of DERs: WT and PV, 2) two types of energy storage systems: electric battery system (EBS) and thermal energy storage (TES), 3) CHP as a power generation unit, as well as 4) MEU consisting of electric boiler (EB), gas boiler (GB), and energy demand for power and heat. The ICES encompasses a singular operator, i.e., ICESO, scheduling energy devices and conducting energy transactions. Specifically, the ICESO can purchase energy from the external energy markets of the wholesale electricity market (WEM) and gas market, and sell to MEUs at self-determined prices.

The ICESO should manage the energy schedules of energy devices and determine the energy prices for MEUs to maximize the total profits. The whole period of operation and transaction can be divided into 24 intervals ($t = \{1, 2, \dots, T\}$), and N MEUs are

represented by $i = \{1, 2, \dots, N\}$. In each time step, the ICESO should read the wholesale prices information, observe the local information of energy devices, and evaluate the state of charge of energy storage systems of TES and EBS before the scheduling. Then, it needs to set the energy prices for MEUs, schedule the operation status of energy devices, and charge or discharge the TES and EBS at each time interval. The detailed models of ICES are presented as follows.

2.1 ICES modeling

2.1.1 Combined heat and power (CHP)

CHP, a single-input multi-output energy converter, assumes a crucial part of the whole ICES due to its high energy conversion efficiency from natural gas to electricity and heat. CHP is characterized by two constant energy conversion efficiencies for electricity and heat. The detailed operation model of CHP, depicted by a non-convex feasible operation region (FOR) enclosed by the boundary curve ABCDEFG, is adopted and shown in Fig.2. The FOR of the CHP is divided into two convex sections and is represented as equations in (1) [21].

$$P_{CHP,n}^t - P_{CHP,n}^B - \frac{P_{CHP,n}^B - P_{CHP,n}^C}{H_{CHP,n}^B - H_{CHP,n}^C} \times (H_{CHP,n}^t - H_{CHP,n}^B) \leq 0, \forall t \in T \quad (1-a)$$

$$P_{CHP}^t - P_{CHP}^C - \frac{P_{CHP}^C - P_{CHP}^D}{H_{CHP}^C - H_{CHP}^D} \times (H_{CHP}^t - H_{CHP}^C) \leq 0, \forall t \in T \quad (1-b)$$

$$-(1 - \bar{X}_{CHP}^t) \times \Gamma \leq P_{CHP}^t - P_{CHP}^E - \frac{P_{CHP}^E - P_{CHP}^F}{H_{CHP}^E - H_{CHP}^F} \times (H_{CHP}^t - H_{CHP}^E), \forall t \in T \quad (1-c)$$

$$-(1 - \underline{X}_{CHP}^t) \times \Gamma \leq P_{CHP}^t - P_{CHP}^D - \frac{P_{CHP}^D - P_{CHP}^E}{H_{CHP}^D - H_{CHP}^E} \times (H_{CHP}^t - H_{CHP}^D), \forall t \in T \quad (1-d)$$

$$\bar{X}_{CHP}^t + \underline{X}_{CHP}^t = I_{CHP}^t, \forall t \in T \quad (1-e)$$

$$-(1 - \underline{X}_{CHP}^t) \times \Gamma \leq H_{CHP}^t - H_{CHP}^E \leq (1 - \bar{X}_{CHP}^t) \times \Gamma, \forall t \in T \quad (1-f)$$

$$0 \leq P_{CHP}^t \leq P_{CHP}^A \times I_{CHP}^t, \forall t \in T \quad (1-g)$$

$$0 \leq H_{CHP}^t \leq H_{CHP}^A \times I_{CHP}^t, \forall t \in T \quad (1-h)$$

In (1), P_{CHP}^t, H_{CHP}^t are generated power and heat for the CHP in time slot t . As the region is described by a non-convex polygon, P_{CHP}^A and H_{CHP}^A indicate the power and heat output of the CHP at point A in the feasible region, and the same applied to the other points BCDEF. $\bar{X}_{CHP}^t(\underline{X}_{CHP}^t)$ states the operating status in the first (second) convex section, when the CHP operate in the first (second) section, $\bar{X}_{CHP}^t(\underline{X}_{CHP}^t) = 1$, and $\underline{X}_{CHP}^t(\bar{X}_{CHP}^t) = 0$. Γ denotes a sufficiently large number to assist model description, while I_{CHP}^t is the commitment status of the CHP. The total operation cost of the CHP unit at time t can be expressed by equation (2), where $a_{CHP}, b_{CHP}, c_{CHP}, d_{CHP}, e_{CHP}$ and f_{CHP} represent the cost coefficients.

$$C_{CHP}^t(P_{CHP}^t, H_{CHP}^t) = a_{CHP}P_{CHP}^t{}^2 + b_{CHP}P_{CHP}^t + c_{CHP} + d_{CHP}H_{CHP}^t{}^2 + e_{CHP}H_{CHP}^t + f_{CHP}P_{CHP}^tH_{CHP}^t \quad (2)$$

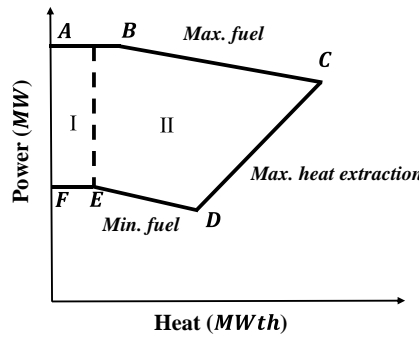


Fig.2. Feasible operation region (FOR) of CHP units

2.1.2 Distributed energy resources (DER)

The power output of DER, denoted as P_{DER}^t , is defined in equation (3) by incorporating the power generation of PV and WT. The power generation function for DER accounts for power output uncertainty, modeled by probabilistic distribution functions for PV and WT, respectively (refer to [30] for detailed modeling).

$$P_{DER}^t = P_{PV}^t + P_{WT}^t \quad (3)$$

As variable renewable energy (VRE), wind power inherently carries high uncertainty. The wind speed (ω), directly influencing power output, is predicted with an unavoidable error $\Delta\omega$ in (4-a). The power output P_{WT}^t of WT is modeled in equation (4-b), where it is positive if and only if the wind speed exceeds the starting speed (ω_{in}^c); otherwise, P_{WT}^t is always zero. The upper limit for WT power is $P_{WT.rated}^t$ when $\omega_{rated}^c \leq \omega \leq \omega_{out}^c$. If the wind speed surpasses the cutout speed ω_{out}^c , WT will be cut out, resulting in $P_{WT}^t = 0$. Additionally, the Weibull probability distribution function (PDF) is employed to estimate the uncertainty parameter due to wind speed prediction errors in (4-c)

$$\omega = \omega_{fs} + \Delta\omega \quad (4-a)$$

$$P_{WT}^t(\omega) = \begin{cases} 0, & \omega \leq \omega_{in}^c \text{ or } \omega \geq \omega_{out}^c \\ \frac{\omega + \omega_{in}^c}{\omega_{rated} + \omega_{in}^c} P_{WT.rated}^t, & \omega_{in}^c \leq \omega \leq \omega_{rated}^c \\ P_{WT.rated}^t, & \omega_{rated}^c \leq \omega \leq \omega_{out}^c \end{cases} \quad (4-b)$$

$$F_\omega(\Delta\omega; \lambda, k) = \begin{cases} \frac{k}{\lambda} \left(\frac{\Delta\omega + 0.5}{\lambda} \right)^{k-1} e^{-\left(\frac{\Delta\omega + 0.5}{\lambda} \right)^k} & \Delta\omega \geq -0.5 \\ 0, & \Delta\omega < -0.5 \end{cases} \quad (4-c)$$

For photovoltaic power generation, this paper introduces the prediction error ΔI of PV in (5-a). PV generates electricity by converting solar radiation energy, and power generation is directly related to solar irradiance in (5-b). The Beta PDF is employed to estimate uncertain parameters with minimal error in (5-c).

$$I = I_{fs} + \Delta I \quad (5-a)$$

$$P_{PV}^t = \sum_{n \in N_{pv}} \eta_{pv_n} S_{pv_n} I^t \quad (5-b)$$

$$F_S(\Delta I; \alpha, \beta) = \frac{(\Delta I + 0.5)^{\alpha-1} (1 - (\Delta I + 0.5))^\beta}{\int_0^1 u^{\alpha-1} (1-u)^\beta du} \quad (5-c)$$

2.1.3 Electric battery system (EBS)

The EBS functions as a charge-dischargeable battery with varying efficiency. The operational strategy of EBS is modeled at a granularity of one hour, i.e., one time interval. Charging and discharging operations are consolidated into a single activity within one time slot. The detailed model of EBS is shown as (6) [31],[32].

$$E_{EBS}^t = (1 - \beta_{EBS}) E_{EBS}^{t-1} + P_{EBS.c}^t \eta_{EBS.c} - P_{EBS.d}^t \quad (6-a)$$

$$0 \leq P_{EBS.c}^t \leq S_{EBS.c}^t P_{EBS.max} \quad (6-b)$$

$$0 \leq P_{EBS.d}^t \leq S_{EBS.d}^t P_{EBS.max} \quad (6-c)$$

$$S_{EBS.c}^t + S_{EBS.d}^t \leq 1 \quad (6-d)$$

$$0 \leq E_{EBS}^t \leq E_{EBS.max} \quad (6-e)$$

In (6), E_{EBS}^t is the battery capacity at time interval t . β and $\eta_{EBS.c}$ are predetermined parameters representing the loss factor and charging efficiency, respectively. $P_{EBS.c}^t$ and $P_{EBS.d}^t$ represents the charging power and discharging power at time step t , respectively. $S_{EBS.c}^t$ and $S_{EBS.d}^t$ represent the charging state and discharging state at time step t , respectively. $P_{EBS.c.max}$ and $P_{EBS.d.max}$ are the maximum charging and discharging power, respectively. $E_{EBS.min}$ and $E_{EBS.max}$ represent the upper and lower limits of battery capacity, respectively.

In the model above, the representation of the state of charge (SoC) is shown in (6-a). The maximal charge and discharge power are constrained by (6-b) and (6-c), respectively. (6-d) is employed to determine the charge of discharge state of EBS. (6-e) constraints the range of total capacity of the energy in EBS.

2.1.4 Thermal energy storage (TES)

A generalized energy storage system model is applied to address TES. This model aligns with that of EBS and is not detailed here for the sake of brevity.

$$E_{TES}^t = (1 - \beta) E_{TES}^{t-1} + H_{TES.c}^t \eta_{TES.c} - H_{TES.d}^t \quad (7-a)$$

$$0 \leq H_{TES.c}^t \leq S_{TES.c}^t H_{TES.max} \quad (7-b)$$

$$0 \leq H_{TES.d}^t \leq S_{TES.d}^t H_{TES.max} \quad (7-c)$$

$$S_{TES.c}^t + S_{TES.d}^t \leq 1 \quad (7-d)$$

$$0 \leq E_{TES}^t \leq E_{TES.max} \quad (7-e)$$

2.2 MEU modeling

As rational integrated energy consumers, MEUs engage in the procurement of energy to fulfil their energy demands for both power and heat. MEUs are conceptualized to possess elastic electricity consumption appliances and energy conversion devices including EB and GB, which enables them to adjust energy consumption dynamically across various time periods and multiple energies.

To encapsulate the utility derived from power consumption for both power and heat, utility functions E_{MEU} and H_{MEU} are conventionally formulated as quadratic functions, as expressed in equations (8) and (9) [8]. This quadratic representation serves as an effective means to capture the nuanced relationship between power consumption and utility over time.

$$E_{MEU}(P_{i,e}^t) = \begin{cases} \omega_i^t - \frac{\lambda_i^t}{2}(P_{i,e}^t)^2, 0 \leq P_{i,e}^t \leq \frac{\omega_i^t}{\lambda_i^t} \\ \frac{(\omega_i^t)^2}{2\lambda_i^t}, P_{i,e}^t > \frac{\omega_i^t}{\lambda_i^t} \end{cases} \quad (8)$$

$$H_{MEU}(H_{i,eb}^t, H_{i,gb}^t, H_{i,h}^t) = -\sigma_i^t(H_{i,eb}^t + H_{i,gb}^t + H_{i,h}^t)^2 + \zeta_i^t(H_{i,eb}^t + H_{i,gb}^t + H_{i,h}^t) \quad (9)$$

In (8), $P_{i,e}^t$ is the power consumption of MEU i during time interval t . ω_i and λ_i are preset parameters reflecting the preference of MEU in energy consumption. In (9), $H_{i,eb}^t$, $H_{i,gb}^t$ and $H_{i,h}^t$ are heat power from EB, GB, and ICES, respectively. Similarly, σ_i^t and ζ_i^t are preset parameters. By considering the utility above, the objective function of MEUs is modelled by (10a) and is constrained by (10-b)-(10-f).

$$\max_{P_{i,e}^t, P_{i,eb}^t, P_{i,gb}^t, H_{i,h}^t} U_{MEU} = \sum_{t=1}^T \left\{ \begin{array}{l} \underbrace{\left(E_{MEU}(P_{i,e}^t) + H_{MEU}(H_{i,eb}^t, H_{i,gb}^t, H_{i,h}^t) \right)}_{\text{Utility for energy consumption}} \\ - \underbrace{\left(x_{r,e}^t(P_{i,e}^t + P_{i,eb}^t) + x_{r,g}^t P_{i,gb}^t + x_{r,h}^t P_{i,h}^t \right)}_{\text{Cost for energy purchase}} \end{array} \right\} \quad (10-a)$$

s. t.

$$H_{i,eb}^t = \eta_{EB,i} P_{i,eb}^t \quad (10-b)$$

$$H_{i,gb}^t = \eta_{GB,i} P_{i,gb}^t \quad (10-c)$$

$$0 \leq P_{i,e}^t \leq P_{i,e}^{t,max} \quad (10-d)$$

$$0 \leq P_{i,eb}^t \leq P_{i,eb}^{t,max} \quad (10-e)$$

$$0 \leq P_{i,gb}^t \leq P_{i,gb}^{t,max} \quad (10-f)$$

In (10), $P_{i,eb}^t$ and $P_{i,gb}^t$ are power and gas consumed by EB and GB of MEU i during time interval t , respectively. $\eta_{EB,i}$ and $\eta_{GB,i}$ are the energy conversion rates of EB and GB for MEU i . $P_{i,e}^{t,max}$, $P_{i,eb}^{t,max}$ and $P_{i,gb}^{t,max}$ are the upper bounds for the corresponding power consumption of electric appliance, power consumption of EB, and gas consumption of GB. (10-a) is the objective function of the MEU with the decision variables of $P_{i,e}^t, P_{i,eb}^t, P_{i,gb}^t, H_{i,h}^t$. In (10-a), the first term is the utility for integrated energy consumption, and the second term is the cost for integrated energy purchase from ICES. Equations (10-b) and (10-c) are the equality constraints for the power conversion of EB and GB. Inequalities (10-d)-(10-f) are constraints for electricity consumption, and power input for EB and GB, respectively.

3. Network Modeling

This section presents the modeling of physical integrated energy networks for electricity, natural gas, and heat within the ICES. These networks are foundational components and are vital for the efficient transmission and distribution of energy resources. Moreover, network constraints that govern the behavior of each network are proposed to comply with physical constraints in real-world operation.

3.1 Electricity distribution network

In the distribution of electricity networks, the prevailing topology is often radial, and it lends itself well to representation as a tree graph. In this representation, the root point corresponds to the connection with the transmission network. The distribution network can thus be visualized as an interconnected web of nodes and transmission lines, embodying the essential structure of a tree graph.

Let $n \in N_e$ denote the set of nodes within the distribution network, and $(n, m) \in P_e$ represent the set of transmission lines governing the interconnection of these nodes. Embracing the paradigm of radial distribution electricity networks, this network configuration captures the hierarchical nature of power flow from the root point, linked to the transmission network, branching out to various nodes within the distribution system. To govern and constrain the dynamics of real power, reactive power, and voltage within the radial distribution network, the linearized DistFlow approach is adopted [33]. The ensuing sections delve into the specifics of how linearized DistFlow constraints shape and guide the real power, reactive power, and voltage considerations in the context of distribution system operation.

$$P_1^t = \sum_{\forall n} x_n^t, t \in T \quad (11 - a)$$

$$P_{n+1}^t = P_n^t - p_{n+1}^t, \forall n \in N_e, t \in T \quad (11 - b)$$

$$Q_{n+1}^t = Q_n^t - q_{n+1}^t, \forall n \in N_e, t \in T \quad (11 - c)$$

$$V_{n+1}^t = V_n^t - (b_n^1 P_n^t + b_n^2 Q_n^t), \forall n \in N_e, t \in T \quad (11 - d)$$

$$\underline{V}_n < V_n^t < \bar{V}_n, \forall n \in N_e, t \in T \quad (11 - e)$$

$$0 \leq p_i^t \leq \bar{p}_i^t, \forall i \in I, t \in T \quad (11 - f)$$

$$0 \leq q_i^t \leq \bar{q}_i^t, \forall i \in I, t \in T \quad (11 - g)$$

$$0 \leq P_{nm}^t \leq \bar{P}_{nm}, \forall n, m \in N_e, \forall (n, m) \in P_e, t \in T \quad (11 - h)$$

$$0 \leq Q_{nm}^t \leq \bar{Q}_{nm}, \forall n, m \in N_e, \forall (n, m) \in P_e, t \in T \quad (11 - i)$$

In (11) P_{nm}^t and Q_{nm}^t indicate the real power and reactive power flow from bus n to node m at time t . V_n^t is the voltage magnitude at the bus n at time t . p_n^t and q_n^t are the real and reactive power exchange at bus n . b_n^1 and b_n^2 are the resistance and reactance between the bus n and $n + 1$. $\bar{V}_n/\underline{V}_n$ are upper/lower bound for voltages of each bus. $\bar{P}_{nm}/\underline{P}_{nm}$ and $\bar{Q}_{nm}/\underline{Q}_{nm}$ denote the upper/lower limits for active and reactive power of the transmission line between bus n and bus m .

3.2 Natural gas network

The natural gas network, renowned for its intricate network of pipelines enabling bidirectional gas flow, constitutes a critical infrastructure for the dissemination of energy resources. Traditionally, the directionality of gas flow is contingent upon the interplay of gas pressure differentials and injections at discrete nodes. However, this paper limits its scope to the dynamics of unidirectional gas flow within this network. This assumption is made upon operational constraints whereby consumers exclusively draw upon gas resources, with the absence of gas production and storage facilities.

Within this defined framework, let $n \in N_g$ denote the set of nodes, and $(n, m) \in P_g$ represent the set of gas pipelines intricately threading through the natural gas network. To model the dynamics of unidirectional gas flow, the study employs the Weymouth equation [34]. The whole network constraints for natural gas networks are given as (12).

$$gf_{mn}^t = \text{sgn}(Pr_n^t, Pr_n^t) C_{mn} \sqrt{|(Pr_n^t)^2 - (Pr_n^t)^2|}, \forall (n, m) \in P_g, \forall t \in T \quad (12 - a)$$

$$-\bar{g}f_{mn} \leq gf_{mn}^t \leq \bar{g}f_{mn}, \forall (n, m) \in P_g \quad (12 - b)$$

$$G_n^t = - \sum_{m \in N_g} gf_{mn}^t, \forall (n, m) \in P_g, \forall t \in T \quad (12 - c)$$

$$\underline{Pr}_n \leq Pr_n^t \leq \bar{Pr}_n, \forall n \in N_g, \forall t \in T \quad (12 - d)$$

$$0 \leq G_n^t \leq \bar{G}_n, \forall n \in N_g, \forall t \in T \quad (12 - e)$$

In (12), gf_{mn}^t is the gas flow in the pipeline from node m to node n . Pr_n^t is the gas pressure of the node n . G_n^t is the gas consumption in the node n . C_{mn} is the line pack constant of gas pipeline mn . $\text{sgn}(\cdot)$ is the signal function to determine the direction of the gas flow [34]. Equations (12a)–(12c) show the constraints for nodal natural gas flow balance with the setting of $P_{REFg,t} = P_{n,max}$. In (12b), $\bar{g}f_{mn}$ is the limitations for the gas flow in the network. Equations (12d)–(12e) limit the nodal pressure and gas sources within its threshold, where \bar{Pr}_n and \underline{Pr}_n are the upper and lower bounds of gas pressure at node n , \bar{G}_n is the limitation for gas consumption in node n . It is worth noting that (12a) is a non-convex equation constraint in an optimization problem, being hard to tackle by using a mathematical programming approach.

3.3 District heating network

Heat networks are vital for transmitting thermal energy through hot water via water pipelines, which are conventionally comprised of supply and return pipelines. The generation of heat energy, typically by CHP systems within the ICES, initiates the flow of water in the supply pipelines to consumers at each node. After the consumer utilizes the heat energy, the water, now cooled, is directed back to the CHP through return pipelines. This unidirectional water flow mirrors the direction of heat flow. Notably, the temperature and pressure of water decrease along the heat transmission direction, indicating both heat loss during transmission and the propulsive force for water flow.

In this paper, Variable Flow Temperature Constant (VFTC) method is employed to model the heating network [35]. The temperature at the supply and return sides of each node is considered constant over time. During heat transmission, a fixed proportion of heat injected into a pipeline is lost as the water progresses to the next node. Denoting nodes as $n \in N_h$ and direct supply and return pipelines as $(n, m) \in S_n^+$ and $(n, m) \in S_n^-$, respectively, the heat network model is formulated as follows.

$$\sum_{(n,m) \in S_n^+} M_{nm}^t - \sum_{(n',m') \in S_n^-} M_{n'm'}^t = M_n^t, \forall (n,m) \in S_n^-, \forall (n',m') \in S_n^+, n \in N_h, \forall t \in T \quad (13-a)$$

$$\sum_{i \in I_n} H_i^t = -c_f M_n^t (T_n^S - T_n^R), n \in N_h, \forall t \in T \quad (13-b)$$

$$\underline{M}_n^N \leq M_n^t \leq \overline{M}_n^N, n \in N_h, \forall t \in T \quad (13-c)$$

$$0 \leq M_{nm}^t \leq \overline{M}_{nm}^S, \forall (n,m) \in (S_n^- \cup S_n^+), \forall t \in T \quad (13-d)$$

In (13), M_{nm}^t represents the pipeline heating flow, m_n^t denotes nodal heating flow, and H_i^t signifies the nodal power injection of a consumer. c_f denotes the heat capacity of water, while T_n^S and T_n^R indicate temperatures of node n in the supply and return networks, respectively. \overline{M}_n^N and \underline{M}_n^N represent the upper and lower bounds of nodal flow. The heat flow \overline{M}_{nm}^S in the pipeline (n,m) is positive if the direction aligns with water flow and negative otherwise. In the proposed model, (13a) is the equality constraints for nodal flow, while (13-b) describes the nodal power injection given the nodal flow. Equations (13c) and (13d) impose inequality constraints on nodal flow and pipeline flow. Importantly, the constraints reveal bidirectional nodal flow and unidirectional water/heat flow within the pipeline.

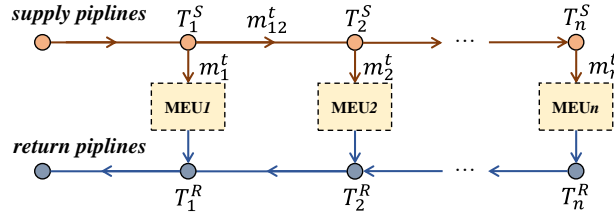


Fig.3. Representation of district heating network

4. Problem formulation

This section presents the multi-networks constrained operational optimization problem for the ICESO and reformulates it into a corresponding C-MDP for the implementation of SRL algorithm. Specifically, the cost term in the C-MDP is denoted by the network constraint violations. By solving this C-MDP, the ICESO can maximize its reward with the tolerated constraint violation.

4.1 Objective function and constraints

The profit of ICESO is mainly the difference between the revenue for selling energy to MEUs and the cost of energy purchasing, as well as the imbalance penalty. The corresponding objective function is presented in (14).

$$\max_{x_{r,e}^t, x_{r,g}^t, x_{r,h}^t} U_{IESP} = \sum_{t=1}^T \left\{ \begin{array}{l} \underbrace{\left(x_{r,e}^t \sum_{i=1}^N P_{i,e}^t + x_{r,g}^t \sum_{i=1}^N P_{i,g}^t + x_{r,h}^t \sum_{i=1}^N P_{i,h}^t \right)}_{\text{Revenue for selling energy}} - \\ \underbrace{\left(x_{w,e}^t P_{w,e}^t + x_{w,g}^t P_{w,g}^t \right)}_{\text{Cost for electricity purchase}} - \underbrace{\left(\delta_e^t P_{imb,e}^t + \delta_g^t P_{imb,g}^t + \delta_h^t H_{imb}^t \right)}_{\text{Cost for energy balance}} \end{array} \right\} \quad (14-a)$$

$$s. t. \forall t \in T$$

$$(1), (2), (3), (4), (5), (6), (7), (11), (12), (13)$$

$$P_{w,e}^t + P_{DER}^t + \sum_{n \in N_e} P_{CHP,n,e}^t + P_{EBS,d}^t - P_{EBS,c}^t + P_{imb,e}^t = \sum_{i \in I_n} P_{i,e}^t \quad (14-b)$$

$$\sum_{n \in N_h} H_{CHP,n}^t + H_{TES,d}^t - H_{EBS,c}^t + H_{imb}^t = \sum_{i \in I_n} H_i^t \quad (14-c)$$

$$P_{w,g}^t + P_{imb,g}^t = \sum_{i \in I_n} P_{i,g}^t + \sum_{n \in N_g} P_{CHP,n,g}^t \quad (14-d)$$

$$x_{min,e}^t \leq x_{r,e}^t \leq x_{max,e}^t \quad (14-e)$$

$$x_{min,g}^t \leq x_{r,g}^t \leq x_{max,g}^t \quad (14-f)$$

$$x_{min,h}^t \leq x_{r,h}^t \leq x_{max,h}^t \quad (14-g)$$

In (14), $\varphi = \{x_{r,e}^t, x_{r,g}^t, x_{r,h}^t, P_{CHP,n,e}^t, P_{EBS,d}^t, P_{EBS,c}^t, H_{CHP,n}^t, H_{TES,d}^t, H_{TES,c}^t\}$ is the set of decision variables, and several decision variables are omitted due to the energy balance among several variables. The objective function in (14-a) constitutes three parts, revenue for selling energy, cost for electricity purchase, and cost for energy balance, where $P_{imb,e}^t, H_{imb}^t, P_{imb,g}^t$ are the imbalanced

electricity, heat and natural gas for ICES operator. Penalty indexes $\delta_e^t, \delta_g^t, \delta_h^t$ are preset parameters to penalize the energy imbalance and determined based on energy prices. Also, the objective is constrained by (1), (2), (3), (4), (9), (10), and (14-b)-(14-g). Equality constraints (14-b)-(14-d) indicate the integrated energy balance. (14e)-(14g) are inequality constraints for the retail energy prices, where $x_{max,e}^t, x_{min,e}^t, x_{max,g}^t, x_{min,g}^t, x_{max,h}^t, x_{min,h}^t$ are preset parameters indicating the upper bounds and lower bounds for power, natural gas and heat, respectively.

The energy balance constraints are actually relaxed by introducing the penalty terms δ . However, network constraints are not directly relaxed to the objective function, as penalties for network constraint violations are hard to determine. Specifically, compared with energy imbalance that only decreases the profits from the economic perspective, the violation of network constraints is more serious and may affect the safe operation of the ICES. Moreover, determining penalties for network constraint violation to realize a fair tradeoff between improving profits and reducing violations is not straightforward. Therefore, it is assumed that the ICES operator aims to guarantee safe operation rather than uplift the economic revenue. Consequently, the network-constrained operational optimization problem is formulated to C-MDP as follows.

4.2 Markov decision process (MDP)

To optimize the decision-making process of ICESO, a MDP is leveraged to describe the integrated energy transactions and then a DRL algorithm is used to solve it. This approach treats the ICESO as an intelligent agent that makes decisions based on the environmental observation of wholesale market prices (both electricity and gas), and power generation of DER. The objective is to improve the pricing decisions by maximizing the accumulated return, using a well-defined reward function in (14-a). The MDP can be denoted by $\langle S, A, R, P, \mu, \gamma \rangle$. S is the set of states. $S = \{x_{w,e}^t, x_{w,g}^t, P_{WT,predict}^t, P_{PV,predict}^t\}$, encompassing electricity market price, natural gas market price, forecast power generation of WT and PV. A is the set of actions. $A = \{x_{r,e}^t, x_{r,g}^t, x_{r,h}^t, P_{CHP}^t, H_{CHP}^t, P_{EBS,c}^t, P_{EBS,d}^t, H_{TES,c}^t, H_{TES,d}^t\}$ represents the available actions as the decision variables in (14-a). $R: S \times A \times S \mapsto \mathbb{R}$ is the reward function, which quantifies the action's performance and is presented by the objective function. $P: S \times A \times S \mapsto [0, 1]$ is the transition probability function. The state transition function is not considered due to the assumption of uncoupled state across time periods. $\mu: S \mapsto P(A)$ represents the policy of the agent, mapping from states to a probability distribution over actions [36]. $\gamma \in [0, 1]$ is the discount factor to discount the future reward.

The discounted accumulative reward under policy μ is denoted as (15). In (15), $\tau = (s_0, a_0, s_1, a_1 \dots)$ is a trajectory of the agent with a series of actions, and $\tau \sim \pi$ indicate trajectories distribution under policy. To conclude, the aim of MDP shown in (16) is to find the optimal policy μ^* that can maximize the discounted accumulative reward $R(\mu)$.

$$R(\mu) = \mathbb{E}_{\tau \sim \pi} \left[\sum_{t=0}^{\infty} \gamma^t R(s_t, a_t, s_{t+1}) \right] \quad (15)$$

$$\mu^* = \arg \max_{\mu} R(\mu) \quad (16)$$

4.3 Constrained-Markov decision process (C-MDP)

To maintain the energy flow complying with the network constraints, a cost function is proposed for the C-MDP, indicating the violation of network constraints. The C-MDP can be denoted as $\langle S, A, R, C, P, \mu, \gamma \rangle$, which is an ordinary MDP augmented by cost function $C(s, a)$. The cost function is denoted by $C: S \times A \times S \mapsto \mathbb{R}$, mapping from transition tuples to cost. The explicit expression of the cost function is given in (17). It comprises the standardized constraint violation of cost in three kinds of network constraints. As the transmission capacity is always designed to be large enough to carry the real and reactive power in the electric distribution network, only voltage constraints are considered in the following cost function.

$$C = \left\{ \begin{array}{l} \underbrace{\sum_{n \in N_e, \forall (n,m) \in P_e} \left[\left[\frac{V_{n,t} - \bar{V}_n}{\bar{V}_n} \right]^+ + \left[\frac{V_n - V_{n,t}}{V_n} \right]^+ \right]}_{\text{Cost for constraints violation in electricity network}} + \\ \underbrace{\sum_{n \in N_g, \forall (n,m) \in P_g} \left[\left[\frac{|gf_{k,mn}| - \bar{g}f_{mn}}{\bar{g}f_{mn}} \right]^+ + \left[\frac{Pr_{k,n} - \bar{P}r_n}{\bar{P}r_n} \right]^+ + \left[\frac{Pr_n - Pr_{k,n}}{\bar{P}r_n} \right]^+ + \left[\frac{G_{k,n} - \bar{G}_n}{\bar{G}_n} \right]^+ \right]}_{\text{Cost for constraints violation in gas network}} + \\ \underbrace{\sum_{n \in N_h, \forall (n,m) \in P_h} \left[\left[\frac{m_n^t - \bar{m}_n^N}{\bar{m}_n^N} \right]^+ + \left[\frac{m_n^N - m_n^t}{\bar{m}_n^N} \right]^+ + \left[\frac{m_{nm}^t - \bar{m}_{nm}^S}{\bar{m}_{nm}^S} \right]^+ \right]}_{\text{Cost for constraints violation in heat network}} \end{array} \right\} \quad (17)$$

In (17), $[x]^+ = \max\{0, x\}$ is the projection function. The cost function is constituting costs for constraint violation in the electricity network, gas network, and heat network. To limit the constraint violation, the constraint for the cost function is proposed as (18), where d is the upper bound of the cost function.

$$C(\mu) \leq d \quad (18)$$

The long-term discounted cost under policy μ is similarly defined as $C(\mu) = E_{\tau \sim \mu}[\sum_{t \in T} \gamma^t C(s_t, a_t, s_{t+1})]$, and the corresponding limit is d . In the C-MDP, the goal is to select a policy μ that maximizes the long-term reward $R(\pi)$ while satisfying the constraints on the long-term costs.

$$\begin{aligned} \mu^* &= \arg \max_{\mu} R(\mu) \\ &s. t. (18) \end{aligned} \quad (19)$$

5. Primal-dual deep deterministic policy gradient (PD-TD3) algorithm

In this section, a PD-TD3 algorithm is developed to solve the proposed C-MDP and learn the optimal operational strategy for ICESO. Specifically, the proposed C-MDP is formulated into a Lagrangian function, which is then converted to an unconstrained min-max problem and thus applicable to the solution of the iterative primal-dual TD3 algorithm. The PD-TD3 algorithm then solves the primal-dual problem by using the gradient descent to iteratively update the policy and Lagrangian multiplier.

5.1 Primal-Dual TD3 algorithm

The challenges of optimal operation of ICES mainly come from the non-linear integrated network constraints. Conventional deep reinforcement learning algorithms do not directly consider these constraints in the learning process [35]. Moreover, traditional DRL algorithms still face the problem of overestimation of Q-value and cost value in C-MDP and instability during the training process. To overcome these drawbacks, the proposed PD-TD3 algorithm is able to address the challenges of network-constrained optimal operation problem in ICES by solving the C-MDP, and mitigating the issue of value overestimation and training instability.

As a RL method, the key of the primal-dual algorithm is to augment constraints on the expected rewards, such that the training of the RL agent converges to the optimal constraints-satisfying policies. Therefore, the objective of primal-dual TD3 for cost minimization can be generally written as (20), where $\mathcal{L}(\mu, \lambda)$ is the augmented objective action-value function, λ denotes the multipliers of constraints.

$$\mathcal{L}(\mu, \lambda) = R(\mu) - \sum_i \lambda(C(\mu) - d) \quad (20)$$

$$(\mu^*, \lambda^*) = \arg \min_{\lambda > 0} \max_{\mu} \mathcal{L}(\mu, \lambda) \quad (21)$$

In (20), $R(\mu)$ and $C(\mu)$ represent the reward and the cost for constraint violation of a DRL agent. For network-constrained optimal operation of ICES, the reward and constraint violation can be the total profits of the ICES and violation of physical constraints of integrated distribution networks, respectively. To solve the unconstrained minimax problem (21), the iterative primal-dual method is used as a canonical approach where in each iteration. In each iteration, the primal policy π and the dual variable λ are updated in turn. The primal-dual update procedures at iteration k are as follows:

$$\theta_{k+1} = \theta_k + \alpha_k \nabla_{\theta} (\mathcal{L}(\mu(\theta), \lambda_k))|_{\theta=\theta_k} \quad (22)$$

$$\lambda_{k+1} = f_k(\lambda_k, \mu(\theta)) \quad (23)$$

In the proposed PD-TD3 algorithm, the primal variable, i.e., policy parameters, is updated by policy gradient, which is specified later. The dual variable, i.e., the Lagrangian multiplier, is updated by (24). In (24), β_k is the step size of the multiplier update. $[x]^+ = \max\{0, x\}$ is the projection onto the dual space $\lambda^k > 0$.

$$\lambda_{k+1} = [\lambda_k + \beta_k (C(\mu_k) - d)]^+ \quad (24)$$

5.2 Algorithm Design for Primal-Dual TD3

The proposed PD-TD3 algorithm is an off-policy DRL algorithm, enabling offline training of strategies in optimization problems and using DNN approximate action-value functions. The overall framework of the PD-TD3 is summarized in Algorithm 1. As a DRL algorithm based on the actor-critic framework, the PD-TD3 adopts DNNs to approximate the value functions and policy functions of the C-MDP, which denotes the critic and actor, respectively. To estimate both the reward and cost in the C-MDP, PD-TD3 employs two kinds of critic networks, namely the reward critic network and the cost critic network. Additionally, as PD-TD3 uses the trick of double Q-learning, each type of critic consists of two online Q networks and their target networks, mitigating the issue of Q-value overestimation observed in other value-based RL algorithms. Also, the target networks of the critic are delayed copies of the online network, which is supposed to mitigate the instability of the training process. Therefore, three sets of neural networks are employed: (1) two reward critic Q-networks $Q_{R1}(s, a | \theta_{R1}^Q)$, $Q_{R2}(s, a | \theta_{R2}^Q)$ and their target network $Q'_{R1}(s, a | \theta_{R1}^{Q'})$,

$Q'_{R2}(s, a|\theta_{R2}^{Q'})$, (2) two cost critic Q-networks $Q_{C1}(s, a|\theta_{C1}^Q)$, $Q_{C2}(s, a|\theta_{C2}^Q)$ and their target networks $Q'_{C1}(s, a|\theta_{C1}^{Q'})$, $Q'_{C2}(s, a|\theta_{C2}^{Q'})$, and (3) the actor policy network $\mu(s|\theta^\mu)$ and its target network $\mu'(s|\theta^{\mu'})$.

During the training process, the agent randomly samples transitions $(s_i, a_i, r_i, c_i, s_{i+1})$ from the experience replay buffer (ERB) to form a mini-batch N for experience replay learning. Then, the target of the reward and cost critic networks are presented as (25) and (26), which are employed to update Q-functions.

$$y_i = r_i + \gamma \min_{j \in \{1,2\}} Q(s_{i+1}, \tilde{a}_{i+1} | \theta_{R_j}^{Q'}) \quad (25)$$

$$z_i = c_i + \gamma \min_{j \in \{1,2\}} Q(s_{i+1}, \tilde{a}_{i+1} | \theta_{C_j}^{Q'}) \quad (26)$$

In (25) and (26), \tilde{a}_{i+1} is the clipped target action shown in (27). Here, target policy smoothing is employed by incorporating clipped Gaussian noise into the target action during the evaluation process. This technique promotes smoother and more stable policy updates, facilitating convergence and enhancing the quality of the learned policy.

$$\tilde{a}_{i+1} = \mu'(s|\theta^{\mu'}) + \tilde{\epsilon}, \tilde{\epsilon} \sim \text{clip}(\mathcal{N}(0, \tilde{\sigma}), -c, c) \quad (27)$$

Based on the target, the reward and cost critic networks are updated by minimizing the loss function, i.e., mean square error (MSE) between the value functions and their targets, proposed in (28) and (29), respectively.

$$L_R = \frac{1}{N} \sum_{i \in N} [y_i - Q_R(s_i, a_i | \theta_R^Q)]^2 \quad (28)$$

$$L_C = \frac{1}{N} \sum_{i \in N} [z_i - Q_C(s_i, a_i | \theta_C^Q)]^2 \quad (29)$$

To mitigate the training error caused by correlated samples, the primal variable, i.e., policy network, and dual variable, i.e., Lagrangian multiplier after a fixed number e of iterations by using (30) and (31), which is the so-called ‘‘delayed’’ update. This delay in primal and dual variable updates reduces the correlation between successive updates and prevents rapid forgetting of previously learned policies. The policy is updated by one step of sampled gradient descent using (30). The Lagrangian multiplier is also updated by using sampled dual gradient in (31). Also, it should be noted that the dual variable updated in (31) uses the minimized estimated Q-value for cost, alleviating the overestimation of the Q value to ensure a proper update descent.

$$\nabla_{\theta^\mu} \mathcal{L}(\theta^\mu, \lambda) \approx \frac{1}{N} \sum_{i \in N} \nabla_{\theta^\mu} [Q_{R1}(s_i, \mu(s_i | \theta^\mu) | \theta_{R1}^Q) - \lambda Q_{C1}(s_i, \mu(s_i | \theta^\mu) | \theta_{C1}^Q)] \quad (30)$$

$$\nabla_{\lambda} \mathcal{L}(\theta^\mu, \lambda) = \frac{1}{N} \sum_{i \in N} [\min_{j \in \{1,2\}} Q(s_{i+1}, \tilde{a}_{i+1} | \theta_{C_j}^{Q'}) - d] \quad (31)$$

Additionally, all target networks of the actor and critic are updated by using the soft update presented in (32) and (33). It allows a small pace update in each iteration and ensures a gradual and stable convergence of the networks, where ρ represents the soft update parameter.

$$\theta^{Q'} \leftarrow \rho \theta_Q + (1 - \rho) \theta^{Q'} \quad (32)$$

$$\theta^{\mu'} \leftarrow \rho \theta_\mu + (1 - \rho) \theta^{\mu'} \quad (33)$$

Algorithm 1 PD-TD3 algorithm

1: Initialize policy parameters θ^μ , Q-function parameters θ_{R1}^Q , θ_{R2}^Q , θ_{C1}^Q , θ_{C2}^Q , and empty buffer R

2: Initialize target networks $\theta^{\mu'} \leftarrow \theta^\mu$, $\theta_{R1}^{Q'} \leftarrow \theta_{R1}^Q$, $\theta_{R2}^{Q'} \leftarrow \theta_{R2}^Q$, $\theta_{C1}^{Q'} \leftarrow \theta_{C1}^Q$, $\theta_{C2}^{Q'} \leftarrow \theta_{C2}^Q$

3: Initialize Lagrangian multiplier λ

4: **repeat**

5: Initialize a random process N for action exploration

6: Receive initial state s_0

7: **for** each transaction time slot $t = 1, \dots, T$ **do**

8: Select action

9: Execute action and observe

10: Store transition in the replay buffer

11: if s is terminal, reset environment state

12: Randomly sample a bath of transitions from N

13: Compute target actions using

$$\tilde{a}_{i+1} = \mu'(s|\theta^{\mu'}) + \tilde{\epsilon}, \tilde{\epsilon} \sim \text{clip}(\mathcal{N}(0, \tilde{\sigma}), -c, c)$$

14: Compute target using

$$y_i = r_i + \gamma \min_{j \in \{1,2\}} Q(s_{i+1}, \tilde{a}_{i+1} | \theta_{R_j}^{Q'})$$

$$z_i = c_i + \gamma \min_{j \in \{1,2\}} Q(s_{i+1}, \tilde{a}_{i+1} | \theta_{C_j}^{Q'})$$

15: Update Q-function by one step of gradient descent by minimizing

$$L_r = \frac{1}{N} \sum_{i \in N} [y_i - Q_r(s_i, a_i | \theta_R^Q)]^2$$

$$L_c = \frac{1}{N} \sum_{i \in N} [z_i - Q_c(s_i, a_i | \theta_C^Q)]^2$$

16: **if** $k \bmod e$ **then**

17: Update policy by one step of gradient ascent using

$$\nabla_{\theta^\mu} \mathcal{L}(\theta^\mu, \lambda) \approx \frac{1}{N} \sum_{i \in N} \nabla_{\theta^\mu} [Q_{R1}(s_i, \mu(s_i | \theta^\mu) | \theta_{R1}^Q) - \lambda Q_{C1}(s_i, \mu(s_i | \theta^\mu) | \theta_{C1}^Q)]$$

18: Update Lagrangian multiplier by one step of gradient ascent using

$$\nabla_{\lambda} \mathcal{L}(\theta^\mu, \lambda) = \frac{1}{N} \sum_{i \in N} [\min_{j \in \{1,2\}} Q(s_{i+1}, \tilde{a}_{i+1} | \theta_{C_j}^{Q'}) - d]$$

19: Update target networks with

$$\theta^{Q'} \leftarrow \rho \theta^Q + (1 - \rho) \theta^{Q'}$$

$$\theta^{\mu'} \leftarrow \rho \theta^\mu + (1 - \rho) \theta^{\mu'}$$

20: **end if**

21: **end for**

22: **until** convergence

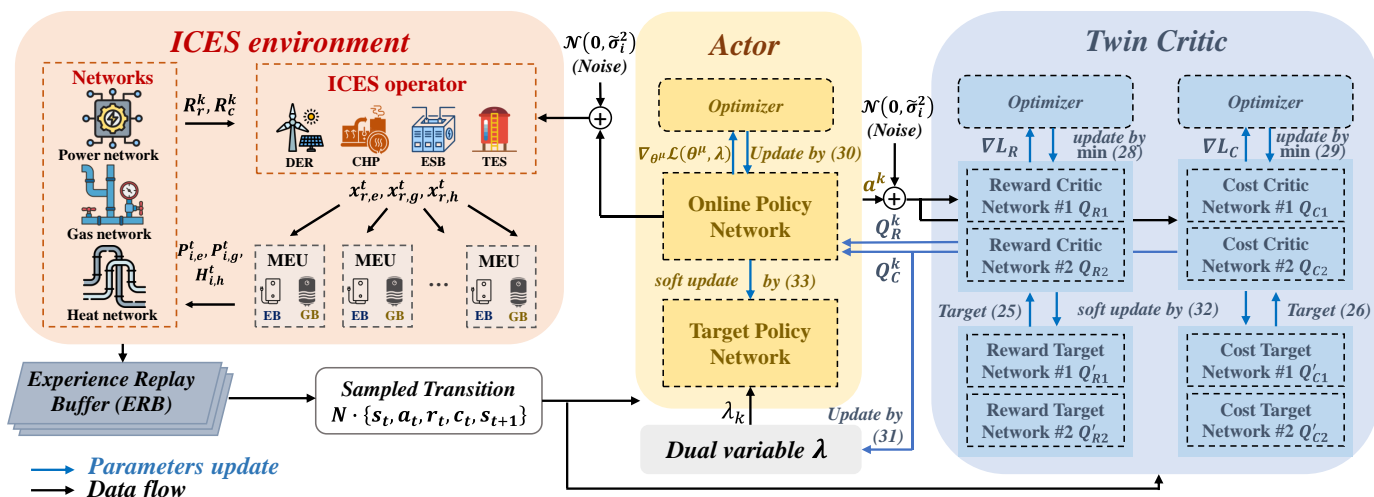


Fig.4. Illustration of the proposed PD-TD3 algorithm

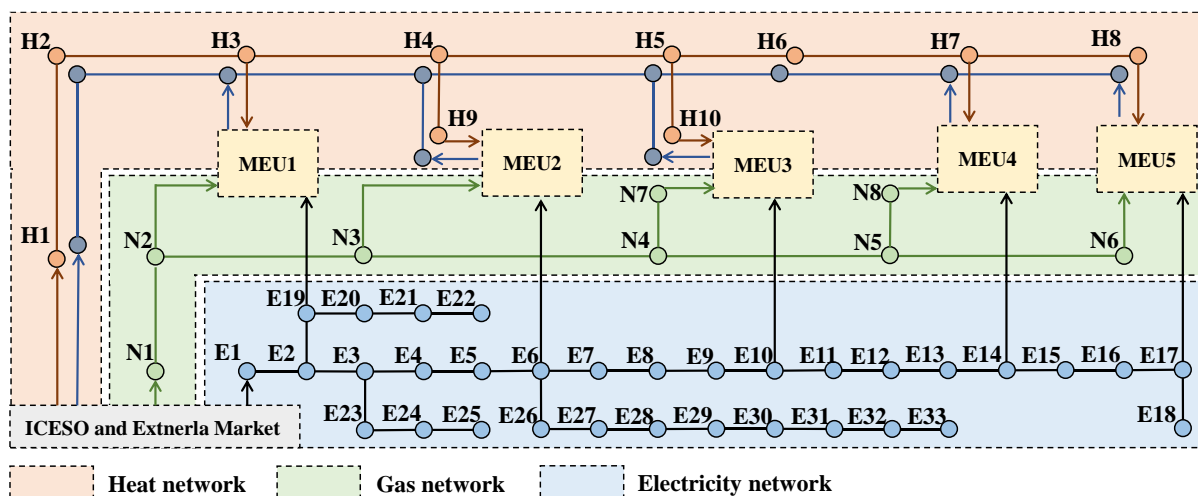


Fig.5. Test case of integrated community energy system

Table 2
Technical specifications of the ICES

Electrical network	$\bar{V}_n = 1.1pu$	$V_n = 0.9pu$	
Natural gas network	$T_g = 288.15K$	$D_g = 0.3m$	$E_g = 90\%$
	$G_g = 0.6N \cdot m^2/kg^2$	$P_g = 101325Pa$	$Z_g = 0.9Pa^{-1}$
	$\bar{P}r_n = 110000Pa$	$\underline{P}r_n = 100000Pa$	$\bar{G}_n = 400m^3/h$
Heating network	$T_{h,max} = 343.15K$	$T_{h,min} = 303.15K$	$c_w = 4200J/(kg \cdot K)$
	$T_{s,loss} = 0.1K/m$	$T_{r,loss} = 0.05K/m$	
Combined heat & power unit	$a_{CHP,n} = 0.0435$	$b_{CHP,n} = 36$	$c_{CHP,n} = 1250$
	$d_{CHP,n} = 0.027$	$e_{CHP,n} = 0.6$	$f_{CHP,n} = 0.011$
	$[P_{CHP}, H_{CHP}] = \{[24,0], [24,8], [10,32], [45,55], [60,16], [60,0]\}$		
Electric battery system	$P_{ba,max} = 0.5MW$	$\eta_{ba} = 0.96$	$\beta_{ba} = 0.01$
	$E_{ba,max} = 2.7MW$	$E_{ba,max} = 0.3MW$	
Thermal energy storage	$H_{sh,max} = 0.7MWt$	$\eta_{sh} = 0.96$	$\beta_{sh} = 0.02$
	$E_{sh,max} = 1.68MWt$	$E_{sh,min} = 0.2MWt$	
Wind turbine	$\omega_{in}^c = 3m/s$	$\omega_{rated}^c = 12m/s$	$\omega_{out}^c = 22m/s$
Photovoltaic	$S_{pv_n} = 500m^2$	$\eta_{pv_n} = 15\%$	

Table 3
Neural network architectures settings

Neutral Networks	Actor	Critic
No. of Hidden Layers	2	2
No. of Neurons	[128,32]	[128,32]
Activation Function	tanh	ReLU
Learning Rate	4e-4	7e-4
Soft update parameter	1e-3	1e-3
Delayed update frequency	2	2
Optimizer	Adam optimizer	Adam optimizer

Table 4
Hyper-parameters settings

Training parameters	Parameters
Replay Buffer Size	1e+6
Replay Start Size	128
Batch Size	128
Discount Factor	0.99

6. Case study

6.1 Simulation setup

In this case study, a test system consisting 5 MEUs is adopted and is shown in Fig.5. As shown in the test system, a standard IEEE-33 bus electricity network, a heat network and a natural gas network are considered to model the whole integrated energy network structure in ICES. The key parameter settings for the test system are given in Table 2. The voltage constraints of the electricity network are set with an upper bound of $0.9p.u.$ and lower bound of $1.1p.u.$, and the other configuration data for the power network is taken from [37]. The natural gas network transmits the gas in the pipeline with an inside diameter of 0.3m and an efficiency of 90%, operating at a temperature of $288.15^\circ K$. The gas compressibility factor is set as $0.9Pa^{-1}$. The allowable pressure for gas transmission is limited from $110kPa$ to $100kPa$, and the maximal gas flow rate is $400m^3/h$. In the 10 node district heat system, the supply temperature at the most upstream node is $70^\circ C$, and the return side temperature of the most downstream node is set to $30^\circ C$. The temperature loss is assumed to be $0.1K/m$ on the supply side, and $0.05K/m$ in return side pipelines [35].

The hourly electricity wholesale prices are obtained from the real-time clearance prices at the UN.EDDY.34.5AMOS node of the New England ISO on April 24, 2023 [38]. The natural gas wholesale prices are based on the average prices in the New England ISO in October 2021 [38]. The constant natural gas price is set at $4.75\text{£}/MMBtu$, resulting in a natural gas price of approximately $16.2\text{£}/MW$ or $0.165\text{£}/m^3$. Moreover, the power output of WT and PV are adapted from real-world data in [39]. The pricing ranges for electricity, natural gas, and heat in the ICES are set as $0 - 50\text{£}/MW$, $0 - 50\text{£}/MW$, and $0 - 40\text{£}/MW$, respectively.

The proposed DRL algorithm is implemented on the Pytorch [40]. The neural networks are configured with the settings shown in Table 3. The hyperparameters of the algorithm shown in Table 4 are selected based on empirical values and adjusted during the training process until the algorithm converges to the maximum profit. The quadratic programming problem for the comprehensive energy demand response of the MEUs is solved using the Gurobi solver [41].

6.2 Training performance

This subsection aims to validate the convergence performance of the PD-TD3. SRL algorithms using both the Lagrangian method and the direct penalty method are employed as benchmark algorithms in the case study. The L-SAC [25] and S-DDPG [28] belong to the former, while typical TD3 with direct penalizing cost stands for the latter. The penalty index λ is set as 1, 10, 100, and 1000 for a comprehensive comparison. In this context, each algorithm is trained 1000 episodes to learn the optimal strategy in pricing and scheduling in ICES, while each episode contains 24 steps, indicating 24 hours per day. Fig.6 and Fig.7 present the evolution of cumulative reward and cost for each episode, respectively. The corresponding values are also listed in Table.5 for a clearer demonstration. The allowable operating range of the cumulative cost is 0~10, and the upper bound of 10 is marked in black in Fig.7.

As illustrated in Fig.6, the cumulative reward of the four algorithms has a similar trend, which fluctuates a lot in the initial stage of training, since the algorithm randomly chooses actions to explore the environment. Similarly, the initial cost for constraint violation in Fig.7 is relatively higher and fluctuates in the initial stage. With the learning process going on, the policy is continuously trained and improved, resulting in an increasing trend in reward and a decreasing trend in cost. In the comparison between the algorithms using the Lagrangian-based method and direct penalty method, it can be observed that typical TD3 algorithms with fixed penalty index usually have lower reward and higher cost. The reward and cost of TD3 decrease as λ increases. Specifically, TD3 with $\lambda = 1000$ has the lowest reward among all algorithms even L-SAC, and the lowest cost among TD3 with all λ settings. Moreover, its cost reaches around the allowable requirement but is still unqualified. This demonstrates a worse performance of the direct penalty-based SRL algorithms compared to Lagrangian-based SRL algorithms.

In the comparison within algorithms using the Lagrangian SRL method, it can be observed that the L-SAC converges with the lowest cumulative reward, which is nearly zero. This is thought as a local optimum and caused by the improper tradeoff between the reward and cost, indicating an over-conservative policy of L-SAC. However, the PD-TD3 shows a fast convergence to the highest reward among the three algorithms, and it can be observed in both Fig.6 and Table.5 that the cumulative reward is about to converge around 200 episodes with a reward of almost 10000. This is driven by the delayed policy update that can update the policy without the training noise, training the policy networks effectively. In addition, the PD-TD3 deals with the physical constraints by directly adjusting the policy of the actor-network. On this account, the cost of PD-TD3 for an episode containing 24 operating hours is in the allowable range of 0~10 after 500 episodes. In comparison, the cost of S-DDPG is out of the allowable range during almost the whole training process, while the cost of L-SAC is about 0 and is thought of as over-conservative. This is owing to the double Q cost networks that assist in estimating the cost more precisely by eliminating the overestimation of cost and thus achieving a fair balancing of the tradeoff between the reward and cost, which has the highest reward and an allowable cost. Furthermore, it can be observed that the reward of PD-TD3 converges around 200 episodes, and the cost is operating in the allowable range after about 500 episodes. The convergence speed of PD-TD3 is similar to L-SAC but is much faster than S-DDPG twice. Also, the convergence process of the reward and cost in PD-TD3 demonstrates that the dual variable converges to optimal after the convergence of reward, since the dual variable is updated with delay in a small step to allow a high exploration in reward, avoiding getting stuck in a local optimum like L-SAC.

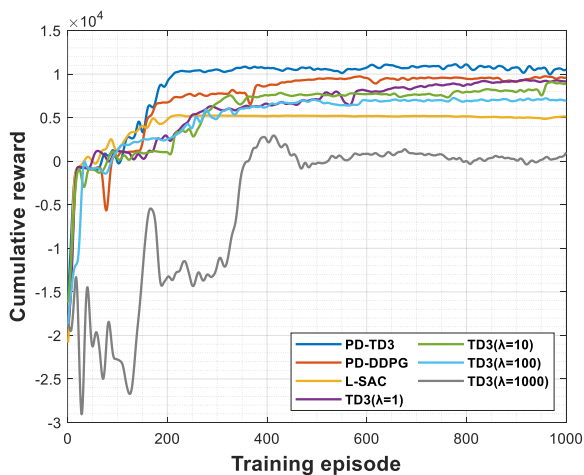


Fig.6. The evolution of cumulative reward for different SRL algorithms.

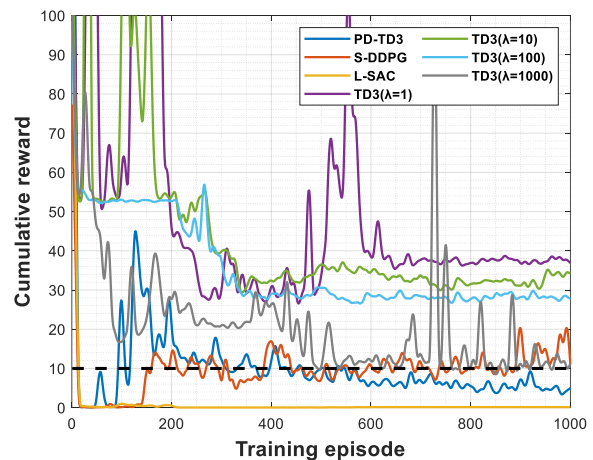


Fig.7. The evolution of cumulative cost of constraint violation for different SRL algorithms.

Table 5

The cumulative values of reward and cost for constraint violation for different SRL algorithms.

Algorithms	Evaluation	Episode						
		1	100	200	400	600	800	1000
PD-TD3	Reward	-15402	-87	9113	10703	11105	10513	10473
	Cost	196	27	21	12	6	5	5
S-DDPG	Reward	-18964	556	6744	8665	9462	9596	9555
	Cost	77	1	14	17	11	10	11
L-SAC	Reward	-20826	1282	4778	5179	5151	5145	5141
	Cost	101	1	0.5	0	0.1	0.1	0.1
TD3 ($\lambda=1$)	Reward	-18965	1151	2786	6593	8794	9162	7412
	Cost	170	60	46	30	38	37	37
TD3 ($\lambda=10$)	Reward	-16229	335	1022	7562	7964	8922	6925
	Cost	126	105	54	32	35	32	34
TD3 ($\lambda=100$)	Reward	-18967	1266	2530	6254	6932	6987	6614
	Cost	96	53	53	29	29	28	28
TD3 ($\lambda=1000$)	Reward	-18964	-22773	-13324	2363	7	1015	6614
	Cost	8990	1830	2102	1993	2072	4210	4471

6.3 Analysis of pricing and operation decisions

For a more in-depth analysis of the learned pricing and device scheduling policies of the three algorithms above, the electricity transactions results for satisfying power demand, electricity dispatch results, and integrated energy transactions results for satisfying heat demand in a test day for comparison of PD-TD3 and S-DDPG without considering conservative results of L-SAC are presented. As illustrated in Fig.8, two transaction results show a similar trend in electricity prices in the whole transaction period because of the inherent impact of the same wholesale electricity prices, but the prices in Fig.8(a) are higher than those in Fig.8(b), therefore resulting in a smoother power consumption curve. The higher prices in Fig.8(a) also lead to a low electric power purchase in WEM in most periods except 11:00-18:00 due to the low power demand and low prices in WEM shown in Fig.9(a). However, the agent of S-DDPG poses a much lower ICES power price, which makes the power consumption curve much steeper. The ICESO of both algorithms determines lower heat prices in periods with a turning on CHP due to its low marginal cost for heat production, while having a lower natural gas price compared to heat in the rest periods.

The devices scheduling is illustrated in Fig.9. It can be observed that the PD-TD3 operates CHP for a longer period and purchases less electricity from the WEM compared to S-DDPG. Specifically, the CHP is turned on during the periods of 0:00-11:00 and 18:00-22:00 to sell power and heat to MEUs, since WEM prices, power, and heat demands are relatively higher. In the rest of the hours, the ICESO tends to sell electricity and natural gas from the external market due to the low demand and high cost of the CHP operation. During some periods, the ICES can provide all the power demand through the power generation from the CHP, DER, and EBS, and the power demand is also cut down or shifted, which is thought of as operating in high energy efficiency. However, the S-DDPG relies on the external market much more by purchasing power and gas to satisfy demand in most periods except for 18:00-22:00, when the CHP is turned on. This is because the S-DDPG algorithm cannot learn the tiny difference in WEM prices and demand between the periods of 0:00-11:00 and 11:00-18:00, even though the market environment during the former periods offers a positive profits uplift for operating the CHP. This not only demonstrates the superior policy of the PD-TD3 compared to S-DDPG but also indicates the high energy efficiency of the ICES operated by the PD-TD3 algorithm.

Nevertheless, the policies generated by the PD-TD3 and S-DDPG also show differences in physical constraint violations. As the power consumption under PD-TD3 is much smoother and lower compared to the S-DDPG shown in Fig.8, it is intuitive that the latter may have more constraint violations in the electrical distribution network due to higher power consumption in peak hours (8:00-9:00 and 18:00-21:00). On the other hand, there is a lower value in a single kind of power consumption for satisfying heat demand in a single time slot, which is operated by S-DDPG and shown in Fig.10. The network safety of gas and heat is easier to guarantee in the former algorithm, while the policy generated by the latter algorithm may transfer the burden of power transmission from the electrical distribution network to the gas and the thermal networks during peak energy consumption periods, which verify the inherent logic of maintaining the operational safety accounting for multi-energy networks.

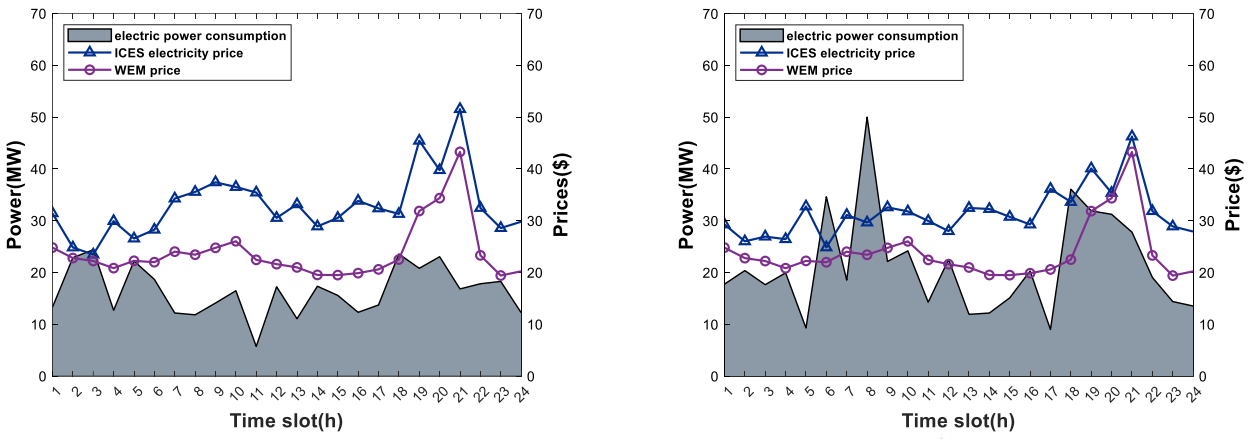


Fig.8. Electricity transaction result with 1) PD-TD3 and 2) S-DDPG

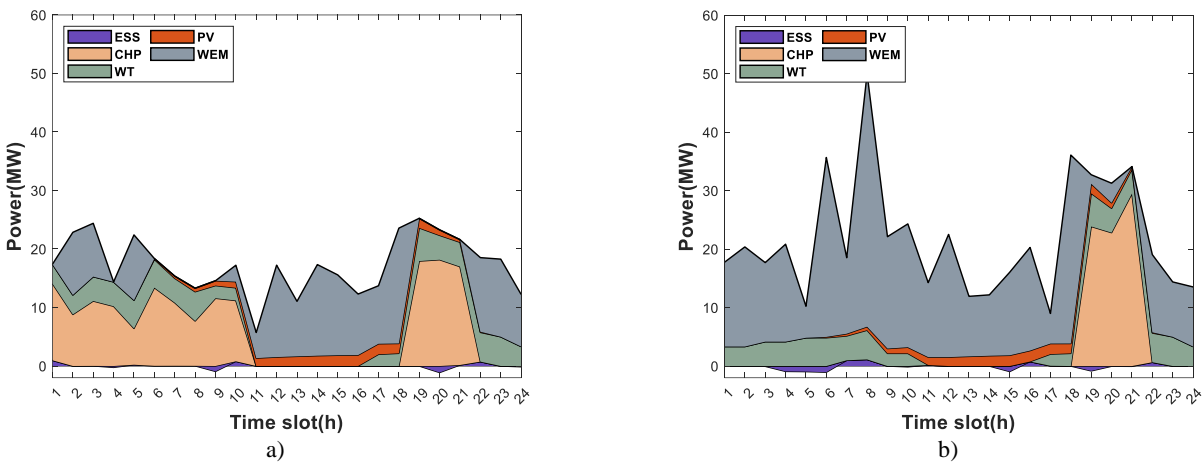


Fig.9. Electricity dispatch results with a) PD-TD3 and b) S-DDPG

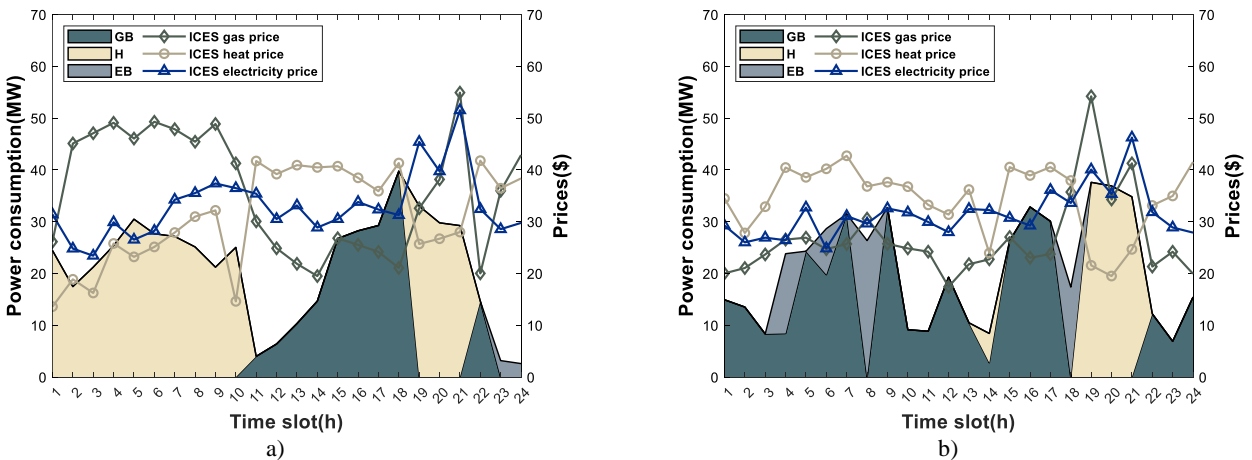


Fig.10. Energy transactions for heat demand with a) PD-TD3 and b) S-DDPG

6.4 Impact of CHP models

As discussed in the section 2.2.1, the CHP with a non-convex operating region is effective in generating both electricity and heat, providing system flexibility in reducing the network constraint violation. This subsection examines the influence of the non-convex CHP model on the operation region. For this purpose, a scenario is constructed using the simplified CHP model with a fixed energy conversion rate. The output is then compared, along with the subsequent impact on energy transactions and ICES operation. The total reward and network constraint violations with different CHP models are presented in Table 2.

In Fig.12, it can be observed that the operation periods of CHP are cut down during 0:00-7:00 since the power and heat output of CHP is constrained leading to it being non-profitable during that period. However, this change also results in higher electricity prices and a different power consumption portfolio with a lower average value in ICES, which is shown in Fig.11. It should be

noted that the less operational profitability of CHP increases the prices for heat but decreases the gas prices, especially during the 0:00-7:00 in Fig.13, when non-convex CHP is in operation but simplified one is not, since the ICESO aims to stimulate the MEUs to consume natural gas instead of heat with turned down CHP. Moreover, the heat consumption is affected even in peak hours of heat demand, which is 18:00-22:00. As the heat generation of CHP is constrained to be linearly related to the power generation, and the heat demand is higher than the power demand during 18:00-22:00, the heat generation is limited to a low level, leading to a significant cut-down in heat consumption in Fig.13 comparing those in Fig.10. Nevertheless, the implementation of simplified CHP model decreases the total generation of both power and heat, which is shown in Table.2. The generations of power and heat decrease around two times and seven times, respective, while the generation cost only decrease no more than three times since the detailed CHP model has a small marginal generation cost for heat. Finally, the implementation of the simplified model results in a lower cumulative reward of 7698.97, compared to 11593.98 in the detailed CHP model.

Even though the simplified model decreases the profits of ICESO significantly, it results in a smaller physical constraint violation of electricity and heat networks and has a similar violation in terms of gas networks in comparison to the detailed one, and is shown in Table.2. Especially, the cost for heat network violation decreases from 4.91 to 0, because of the significant decrease in heat generation of CHP and the consequent reduced heat consumption of MEUs. On the other hand, due to the substitute effect, MEUs tend to consume more natural gas, putting a burden on the gas network operation. This leads to a slightly higher cost for gas network constraint violations. In summary, the implementation of a simplified model cut down the power and heat generation, and cumulative reward significantly by narrowing the operation region, indicating that the simplified model deviates from the detailed model to a great extent and reflects an unfaithful simulation of the ICES operation in reality.

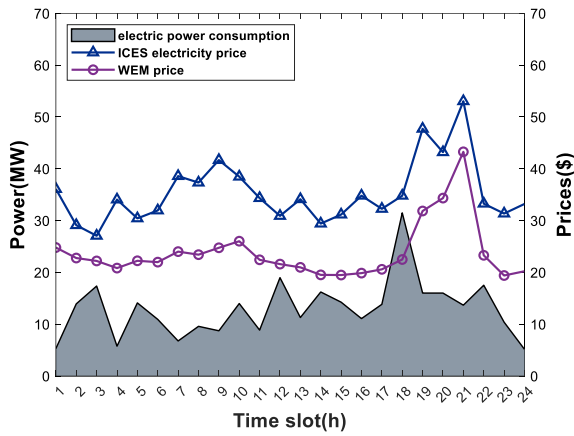


Fig.11. Electricity transaction result with simplified CHP

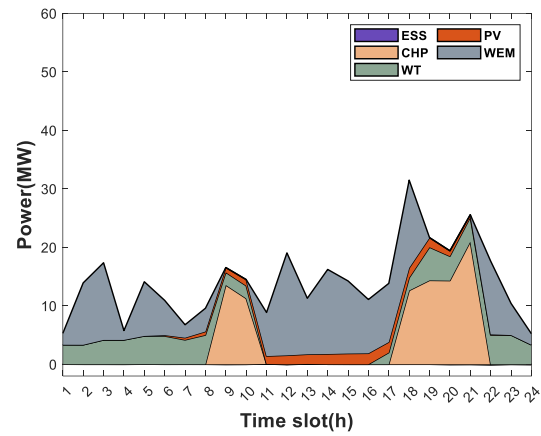


Fig.12. Electricity devices dispatch with simplified CHP

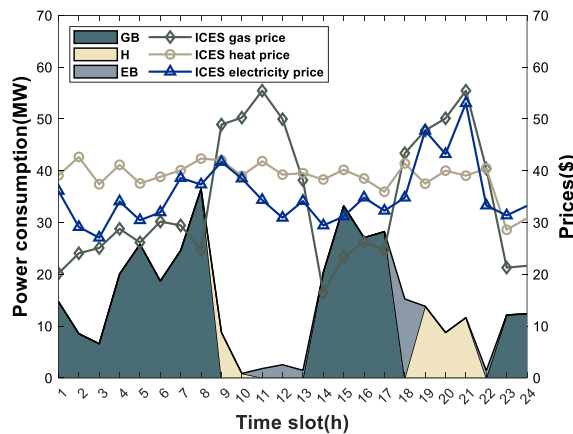


Fig.13. Energy transactions for heat demand with simplified CHP

Table 6
Results comparison of implementing detailed and simplified CHP models

	Total reward	Network violation			CHP output		
		E	G	H	E	H	Cost
Detailed CHP model with non-convex feasible region	11593.98	0.65	0.10	4.91	163.61	501.25	5728.65
Simplified CHP model with fixed conversion rate	7698.97	0.56	0.20	0.00	87.04	69.63	2558.4

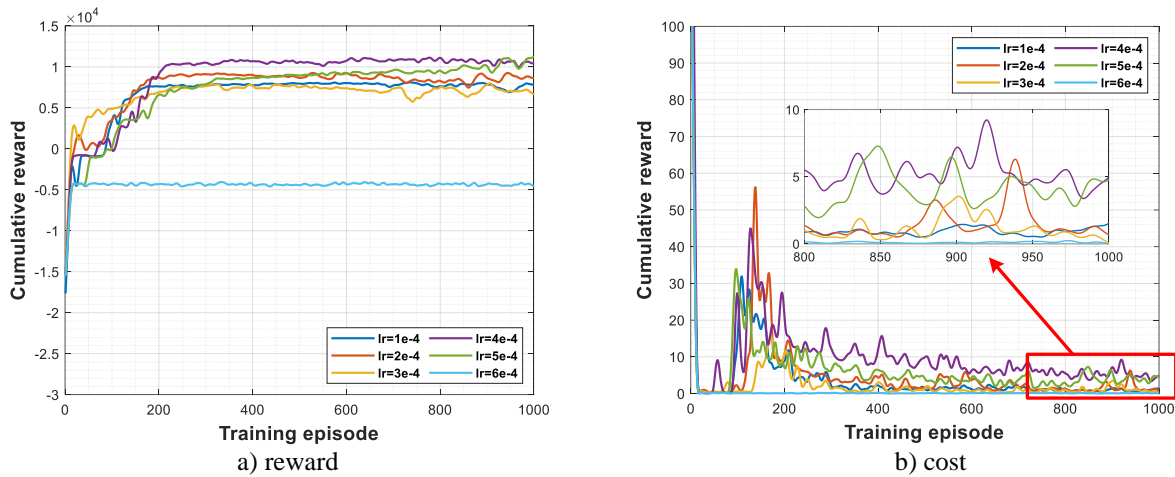


Fig.14. Evolution of cumulative reward and cost under different actor network (policy) learning rate

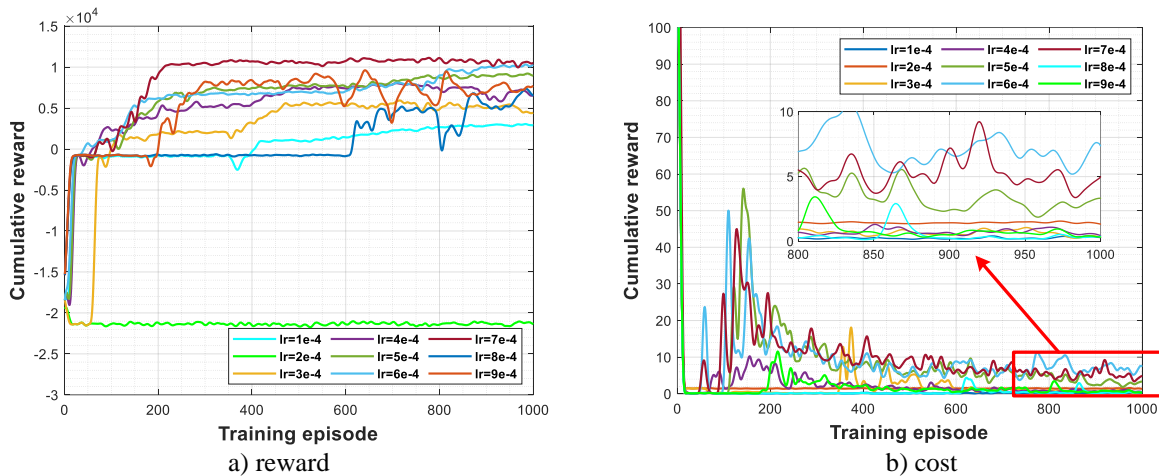


Fig.15. Evolution of cumulative reward and cost under different critic network (Q-value) learning rate

6.5 Sensitivity analysis

As hyperparameters have a great impact on algorithm performance, sensitivity analysis is conducted on selected hyperparameters, mainly including the Q-network learning rate and actor-network learning rate. Fig.14 shows the evolution of cumulative reward and cost under different actor-network (policy) learning rates. It can be observed in Fig.14 a) that the episode reward can converge to a high value fast with a learning rate lying from $1e-4$ to $5e-4$ but may converge to a low value, which is a local optimal, in several episodes with a policy learning rate from $6e-4$. Also, the curve of the cumulative reward increases faster in the initial stage with a lower learning rate in policy, which means the exploration in the initial stage contains a higher proportion of useless stochastic noise compared to the later stage. Among these parameter settings, the policy learning rate of $4e-4$ (purple) can assist in achieving the highest accumulative reward. When comparing Fig.14 a) with b), the policy learning rate with a higher cumulative reward always results in a higher cost for constraint violation. This demonstrates that the converged cumulative reward has a positive correlation with the cumulative cost, while the policy learning rate plays a key role in the tradeoff of the reward and cost. As all of these parameter settings satisfy the safe operating range of $0 \sim 10$, the policy learning rate with the highest cumulative reward, which is $4e-4$, is selected to be the final setting of the algorithm.

As for the critic network learning rate shown in Fig.15, the converged reward, as well as the cost, firstly increases and then decreases with the growing actor-network learning rate, and the learning rate of $7e-4$ shows the highest cumulative reward. In general, the evolution curve with a lower learning rate tends to increase gently, while it shows a steep increase or decrease in reward and cost with a higher learning rate. Moreover, a positive correlation between the reward and cost can also be observed for different settings in Fig.15. Interestingly, the cumulative cost with the learning rate of $5e-4$ and $6e-4$ may exceed the tolerated cost during the training process, while the cost curve with $8e-4$ is nearly zero and is considered too conservative. Among these parameter settings of the critic learning rate, the settings of $7e-4$ can balance the reward and cost and increase the algorithm performance to the greatest extent.

7. Conclusion

In conclusion, this paper presents the development of the PD-TD3 algorithm to solve the constrained operational optimization problem in ICES. The algorithm is an SRL algorithm based on the Lagrangian method, utilizing a Lagrangian multiplier to penalize the constraint violation during the policy updates. Furthermore, double Q networks are employed to mitigate the Q value over-estimation issue of both reward and cost, enabling accurate updates of the Lagrangian multiplier and achieving a balanced tradeoff between the reward and cost. The paper analyzes the optimal strategy in operation and pricing, as well as the convergence performance of multiple algorithms, demonstrating the superior performance of the proposed algorithm in finding the optimal strategy. Additionally, the paper reveals that the non-convex model of CHP significantly differs and can attain a higher economic value than the CHP with the fixed energy conversion rate. Future work is planned to extend this research to the low carbon dispatch problem by considering carbon emission trading in ICES, a crucial step in reducing carbon emissions and promoting the energy transition on the demand side.

Reference

- [1] Chang, M., Thellufsen, J. Z., Zakeri, B., Pickering, B., Pfenninger, S., Lund, H., & Østergaard, P. A. (2021). Trends in tools and approaches for modelling the energy transition. *Applied Energy*, 290, 116731-.
- [2] Li, P., Li, S., Yu, H., Yan, J., Ji, H., Wu, J., & Wang, C. (2022). Quantized event-driven simulation for integrated energy systems with hybrid continuous-discrete dynamics. *Applied Energy*, 307, 118268-.
- [3] IEA. 2020 global status report for buildings and construction. International Energy Agency 2020.
- [4] Lv, C., Yu, H., Li, P., Wang, C., Xu, X., Li, S., & Wu, J. (2019). Model predictive control based robust scheduling of community integrated energy system with operational flexibility. *Applied Energy*, 243, 250–265.
- [5] Sun, Q., Wang, X., Liu, Z., Mirsaedi, S., He, J., & Pei, W. (2022). Multi-agent energy management optimization for integrated energy systems under the energy and carbon co-trading market. *Applied Energy*, 324, 119646-.
- [6] Koirala, B. P., Koliou, E., Friege, J., Hakvoort, R. A., & Herder, P. M. (2016). Energetic communities for community energy: A review of key issues and trends shaping integrated community energy systems. *Renewable and Sustainable Energy Reviews*, 56, 722-744.
- [7] Fontenot, H., & Dong, B. (2019). Modeling and control of building-integrated microgrids for optimal energy management – A review. *Applied Energy*, 254, 113689-.
- [8] Bahrami, S., & Sheikhi, A. (2016). From Demand Response in Smart Grid Toward Integrated Demand Response in Smart Energy Hub. *IEEE Transactions on Smart Grid*, 7(2), 650–658.
- [9] Li, P., Wang, Z., Wang, N., Yang, W., Li, M., Zhou, X., Yin, Y., Wang, J., & Guo, T. (2021). Stochastic robust optimal operation of community integrated energy system based on integrated demand response. *International Journal of Electrical Power & Energy Systems*, 128, 106735-.
- [10] Wang, L., Hou, C., Ye, B., Wang, X., Yin, C., & Cong, H. (2021). Optimal Operation Analysis of Integrated Community Energy System Considering the Uncertainty of Demand Response. *IEEE Transactions on Power Systems*, 36(4), 3681–3691.
- [11] Li, Y., Han, M., Yang, Z., & Li, G. (2021). Coordinating Flexible Demand Response and Renewable Uncertainties for Scheduling of Community Integrated Energy Systems With an Electric Vehicle Charging Station: A Bi-Level Approach. *IEEE Transactions on Sustainable Energy*, 12(4), 2321–2331.
- [12] Li, Y., Wang, B., Yang, Z., Li, J., & Li, G. (2022). Optimal Scheduling of Integrated Demand Response-Enabled Community-Integrated Energy Systems in Uncertain Environments. *IEEE Transactions on Industry Applications*, 58(2), 2640–2651.
- [13] Li, Y., Han, M., Shahidehpour, M., Li, J., & Long, C. (2023). Data-driven distributionally robust scheduling of community integrated energy systems with uncertain renewable generations considering integrated demand response. *Applied Energy*, 335, 120749-.
- [14] Chen, Y., Wei, W., Liu, F., & Mei, S. (2017). A multi-lateral trading model for coupled gas-heat-power energy networks. *Applied Energy*, 200, 180–191.
- [15] Yao, W., Wang, C., Yang, M., Wang, K., Dong, X., & Zhang, Z. (2023). A tri-layer decision-making framework for IES considering the interaction of integrated demand response and multi-energy market clearing. *Applied Energy*, 342, 121196-.
- [16] Zhou, C., Jia, H., Jin, X., Mu, Y., Yu, X., Xu, X., Li, B., & Sun, W. (2023). Two-stage robust optimization for space heating loads of buildings in integrated community energy systems. *Applied Energy*, 331, 120451-.
- [17] Rong, A., & Lahdelma, R. (2007). An efficient envelope-based Branch and Bound algorithm for non-convex combined heat and power production planning. *European Journal of Operational Research*, 183(1), 412-431.
- [18] Mendes, G., Ioakimidis, C., & Ferrão, P. (2011). On the planning and analysis of Integrated Community Energy Systems: A review and survey of available tools. *Renewable and Sustainable Energy Reviews*, 15(9), 4836-4854.
- [19] Silver, D., Huang, A., Maddison, C. J., Guez, A., Sifre, L., Van Den Driessche, G., Schrittwieser, J., Antonoglou, I., Panneershelvam, V., Lanctot, M., Dieleman, S., Grewe, D., Nham, J., Kalchbrenner, N., Sutskever, I., Lillicrap, T., Leach, M., Kavukcuoglu, K., Graepel, T., & Hassabis, D. (2016). Mastering the game of Go with deep neural networks and tree search. *Nature (London)*, 529(7587), 484–489.
- [20] Mnih, V., Kavukcuoglu, K., Silver, D., Graves, A., Antonoglou, I., Wierstra, D., & Riedmiller, M. (2013). Playing Atari with Deep Reinforcement Learning. *ArXiv.Org*.

- [21] Dolatabadi, A., Abdeltawab, H., & Mohamed, Y. A.-R. I. (2023). A Novel Model-Free Deep Reinforcement Learning Framework for Energy Management of a PV Integrated Energy Hub. *IEEE Transactions on Power Systems*, 38(5), 4840–4852.
- [22] Li, Y., Bu, F., Li, Y., & Long, C. (2023). Optimal scheduling of island integrated energy systems considering multi-uncertainties and hydrothermal simultaneous transmission: A deep reinforcement learning approach. *Applied Energy*, 333, 120540-.
- [23] Li, H., & He, H. (2022). Learning to operate distribution networks with safe deep reinforcement learning. *IEEE Transactions on Smart Grid*, 13(3), 1860-1872.
- [24] Wang, B., Li, Y., Ming, W., & Wang, S. (2020). Deep Reinforcement Learning Method for Demand Response Management of Interruptible Load. *IEEE Transactions on Smart Grid*, 11(4), 3146–3155.
- [25] Wang, W., Yu, N., Gao, Y., & Shi, J. (2020). Safe Off-Policy Deep Reinforcement Learning Algorithm for Volt-VAR Control in Power Distribution Systems. *IEEE Transactions on Smart Grid*, 11(4), 3008–3018.
- [26] Chow, Y., Ofir Nachum, Faust, A., Duenez-Guzman, E., & Ghavamzadeh, M. (2019). Lyapunov-based Safe Policy Optimization for Continuous Control. *ArXiv.Org*.
- [27] Sayed, A. R., Zhang, X., Wang, Y., Wang, G., Qiu, J., & Wang, C. (2023). Online Operational Decision-making for Integrated Electric-Gas Systems with Safe Reinforcement Learning. *IEEE Transactions on Power Systems*, 1–14.
- [28] Qiu, D., Dong, Z., Zhang, X., Wang, Y., & Strbac, G. (2022). Safe reinforcement learning for real-time automatic control in a smart energy-hub. *Applied Energy*, 309, 118403-.
- [29] Yan, Z., & Xu, Y. (2022). A Hybrid Data-driven Method for Fast Solution of Security-Constrained Optimal Power Flow. *IEEE Transactions on Power Systems*, 37(6), 1–1.
- [30] Fazlalipour, P., Ehsan, M., & Mohammadi-Ivatloo, B. (2019). Risk-aware stochastic bidding strategy of renewable microgrids in day-ahead and real-time markets. *Energy (Oxford)*, 171, 689–700.
- [31] Long, Y., Li, Y., Wang, Y., Cao, Y., Jiang, L., Zhou, Y., Deng, Y., & Nakanishi, Y. (2022). Low-carbon economic dispatch considering integrated demand response and multistep carbon trading for multi-energy microgrid. *Scientific Reports*, 12(1), 6218–6218.
- [32] Xiao, D., Lin, Z., Chen, H., Hua, W., & Yan, J. (2024). Windfall profit-aware stochastic scheduling strategy for industrial virtual power plant with integrated risk-seeking/averse preferences. *Applied Energy*, 357. <https://doi.org/10.1016/j.apenergy.2023.122460>
- [33] Yang, T., Guo, Y., Deng, L., Sun, H., & Wu, W. (2021). A Linear Branch Flow Model for Radial Distribution Networks and Its Application to Reactive Power Optimization and Network Reconfiguration. *IEEE Transactions on Smart Grid*, 12(3), 2027–2036.
- [34] Xu, D., Wu, Q., Zhou, B., Li, C., Bai, L., & Huang, S. (2020). Distributed Multi-Energy Operation of Coupled Electricity, Heating, and Natural Gas Networks. *IEEE Transactions on Sustainable Energy*, 11(4), 2457–2469.
- [35] Frölke, L., Sousa, T., & Pinson, P. (2022). A network-aware market mechanism for decentralized district heating systems. *Applied Energy*, 306, 117956-.
- [36] Liang, Q., Que, F., & Modiano, E. (2018). Accelerated Primal-Dual Policy Optimization for Safe Reinforcement Learning. *ArXiv.Org*.
- [37] Dolatabadi, S. H., Ghorbanian, M., Siano, P., & Hatzigargyriou, N. D. (2021). An Enhanced IEEE 33 Bus Benchmark Test System for Distribution System Studies. *IEEE Transactions on Power Systems*, 36(3), 2565–2572.
- [38] ISO England. (2023). Information on individual iso markets, market products, and ancillary services. <https://www.iso-ne.com/markets-operations/markets/>
- [39] Ajoulabadi, A., Ravadanegh, S. N., & Behnam Mohammadi-Ivatloo. (2020). Flexible scheduling of reconfigurable microgrid-based distribution networks considering demand response program. *Energy (Oxford)*, 196, 117024-.
- [40] Paszke, A., Gross, S., Massa, F., Lerer, A., Bradbury, J., Chanan, G., Killeen, T., Lin, Z., Gimelshein, N., Antiga, L., Desmaison, A., Köpf, A., Yang, E., DeVito, Z., Raison, M., Tejani, A., Chilamkurthy, S., Steiner, B., Lu, F., ... Chintala, S. (2019). PyTorch: An Imperative Style, High-Performance Deep Learning Library. *ArXiv.Org*.
- [41] Gurobi Optimization, LLC. (2023). Gurobi Optimizer Reference Manual. <https://www.gurobi.com/>